Effects of anisotropy in spin molecular-orbital coupling on effective spin models of trinuclear organometallic complexes

J. Merino
Departamento de Física Teórica de la Materia Condensada, Condensed Matter Physics Center (IFIMAC) and Instituto Nicolás Cabrera, Universidad Autónoma de Madrid, E-28049 Madrid, Spain

A. C. Jacko, A. L. Khosla, and B. J. Powell
School of Mathematics and Physics, The University of Queensland, Brisbane, Queensland 4072, Australia
(Received 24 March 2017; revised manuscript received 27 September 2017; published 10 November 2017)

We consider layered decorated honeycomb lattices at two-thirds filling, as realized in some trinuclear organometallic complexes. Localized $S = 1$ moments with a single-spin anisotropy emerge from the interplay of Coulomb repulsion and spin molecular-orbit coupling (SMOC). Magnetic anisotropies with bond-dependent exchange couplings occur in the honeycomb layers when the direct intracluster exchange and the spin molecular-orbital coupling are both present. We find that the effective spin exchange model within the layers is an XXZ + 120° honeycomb quantum compass model. The intrinsic nonspherical symmetry of the multinuclear complexes leads to very different transverse and longitudinal spin molecular-orbital couplings, which greatly enhances the single-spin and exchange coupling anisotropies. The interlayer coupling is described by an XXZ model with anisotropic biquadratic terms. As the correlation strength increases the system becomes increasingly one-dimensional. Thus, if the ratio of SMOC to the interlayer hopping is small this stabilizes the Haldane phase. However, as the ratio increases there is a quantum phase transition to the topologically trivial "D phase." We also predict a quantum phase transition from a Haldane phase to a magnetically ordered phase at sufficiently strong external magnetic fields.

DOI: 10.1103/PhysRevB.96.205118

I. INTRODUCTION

The interplay of strong Coulomb interaction and spin-orbit coupling (SOC) can lead to emergent quantum phases [1] and new phenomena which remain poorly understood. The conventional Mott transition can be strongly affected by SOC leading to a topological Mott insulator with bulk charge gap but fractionalized surface states carrying spin but no charge [2]. Such states may be realized in Ir-based transition metal oxides such as Sr_2IrO_4. In contrast to conventional Mott insulators, the spin exchange interactions arising in Mott insulators with SOC are typically anisotropic with quantum compass [3] instead of the conventional Heisenberg interactions. A possible realization of a quantum compass model on a hexagonal lattice, i.e., a Heisenberg-Kitaev model [4–6], may be found in Na_2IrO_3 and Li_2IrO_3 materials in which SOC removes the orbital degeneracy of the 5d electrons leading to effective $S = 1/2$ pseudospins. Interestingly, the Kitaev model is exactly solvable: It sustains a spin liquid ground state whose low-energy excitations are Majorana fermions [7]. In other iridates with strong SOC such as Sr_2IrO_4, an antisymmetric Dzyaloshinski-Moriya (DM) interaction arises associated with the lack of an inversion symmetry center.

There are several strongly correlated molecular materials in which spin-orbit coupling is relevant including, metal-organic frameworks [8], layered organic salts [9,10], and multinuclear coordinated organometallic complexes [11–15]. The elementary building blocks of multinuclear complexes are molecular clusters containing transition metal ions whose d orbitals are hybridized with molecular orbitals where each of the hybrids is typically described by a single Wannier orbital [16]. The coupling of the spin with the electron currents around the Wannier orbitals describing each molecule gives rise to a spin molecular-orbital coupling (SMOC) [12,13].

A typical multinuclear complex is $Mo_3S_7(dmit)_3$. Here the honeycomb networks of $Mo_3S_7(dmit)_3$ molecules are stacked on top of each other along the c direction of the crystal. $Mo_3S_7(dmit)_3$ molecules can be described by three Wannier orbitals [16], and their packing on a honeycomb lattice within the layers leads to a decorated honeycomb lattice, as shown in Fig. 1. The electronic and magnetic properties of the decorated honeycomb lattice are interesting both in the weakly and strongly interacting limit. At weak coupling, a tight-binding model on such a lattice leads to topological insulating phases when SOC is turned on which displays the quantum spin hall effect [17] as predicted in graphene [18]. At strong coupling, the exact ground state of the Kitaev model on the decorated honeycomb lattice [19], is a chiral spin liquid. Therefore, it is interesting to find possible realizations of the decorated honeycomb lattice in actual materials to probe such rich physics. Furthermore, similar models arise naturally in a number of other organic [10] and organometallic materials [11,20–23] and inorganic compounds with decorated lattices [24–26].

Organometallic complexes have intrinsic structural properties which make them different to transition metal oxides. A crucial difference comes from the fact that isolated molecular clusters break the spherical symmetry present in isolated transition metal ions. While the total angular momentum of the ion is conserved, it is only the component perpendicular to the molecular plane that is conserved in cyclic molecular clusters. Hence, in these systems, anisotropies are intrinsic to the molecules constituting the material, whereas in transition

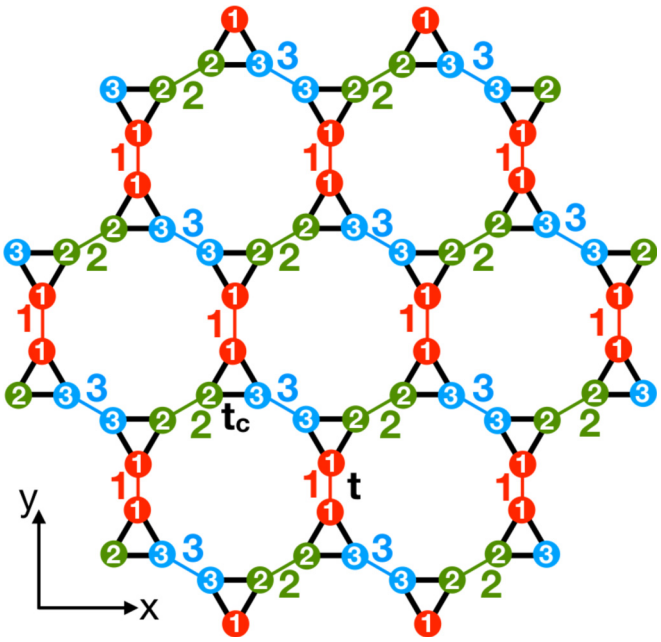

FIG. 1. The decorated honeycomb lattice realized in the a-b planes of $Mo_3S_7(dmit)_3$ crystals. The small triangles represent the organometallic trinuclear clusters located at sites of the honeycomb lattice. The intracluster hopping t_c, and the intercluster hopping t, entering our model (2) are also shown. Note the labeling (color coding) of both the sites within the trinuclear clusters and the intracluster t bonds. The full crystal consists of these decorated honeycomb layers stacked along the c direction; see Fig. 2(b).

metal oxides anisotropies can only be achieved via the environment surrounding the ions in the crystal. This suggests that anisotropic spin exchange interactions may be easily generated in organometallic complexes due to their intrinsic structure. These anisotropies may be further enhanced by the anisotropic SMOC typically found in these systems [13,15]. SMOC is an emergent coupling between electron currents circulating around the cyclic molecules and the electron spin. Also by tuning the relative orientation between molecules in the crystal a Dzyaloshinskii-Moriya interaction can be generated [15]. All the above suggests that these materials are ideal playgrounds for the realization of quantum compass models [3].

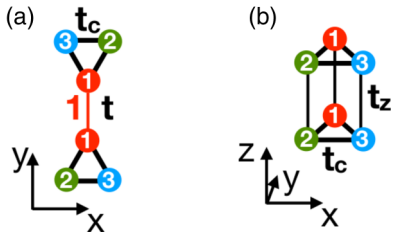

FIG. 2. The two arrangements of two neighbor trimers relevant to $Mo_3S_7(dmit)_3$ crystals. In (a) we show two neighbor trimers in the a-b plane whereas in (b) the two trimers are stacked along the c direction. In the dumbbell arrangement (a) the two molecules are related by inversion symmetry through the midpoint of the bond while in the tube arrangement (b) they are related by translational symmetry.

Recently [14,15] we derived an effective superexchange Hamiltonian that captures the magnetic properties of trinuclear coordinated complexes at strong coupling. The onsite Coulomb repulsion U leads to $S=1$ moments localized at each triangular cluster from which SMOC, λ, induces a single-spin anisotropy D. The $S=1$ moments behave as weakly coupled chains due to the decorated lattice structure of trinuclear organometallic complexes [14,15]. The lattice structure is such that three hopping amplitudes connect two nearest-neighbor molecules along the c direction while only one hopping amplitude connects nearest-neighbor molecules in the a-b planes; cf. Fig. 2. As U is increased exchange of electrons between nearest-neighbor molecules in the a-b plane is suppressed as compared to exchange between molecules along the c direction. This leads to a quasi-one-dimensional effective spin exchange model of $S=1$ localized moments which is in the Haldane phase [15].

Here we extend our previous work, which focused on $Mo_3S_7(dmit)_3$, by studying the more general problem of trinuclear organometallic complexes with strong correlations and strong anisotropic SMOC. After introducing our general combined analytical and numerical approach to extract exchange coupling parameters in these systems we show how anisotropy in SMOC plays a crucial role in determining the level of anisotropy of the effective spin Hamiltonian. We show that the effective spin exchange Hamiltonian for two-thirds filled trinuclear coordination crystals is

$$H_{\rm eff} = D^* \sum_{\ell} (\mathcal{S}^z_{\boldsymbol{r}_\ell})^2 + J^c \sum_{\ell} \left(\mathcal{S}^x_{\boldsymbol{r}_\ell} \mathcal{S}^x_{\boldsymbol{r}_\ell+\boldsymbol{\delta}_z} + \mathcal{S}^y_{\boldsymbol{r}_\ell} \mathcal{S}^y_{\boldsymbol{r}_\ell+\boldsymbol{\delta}_z} + \Delta^c \mathcal{S}^z_{\boldsymbol{r}_\ell} \mathcal{S}^z_{\boldsymbol{r}_\ell+\boldsymbol{\delta}_z} \right) + \sum_{\ell\alpha\beta} P_{\alpha\beta} \mathcal{S}^\alpha_{\boldsymbol{r}_\ell} \mathcal{S}^\beta_{\boldsymbol{r}_\ell} \mathcal{S}^\alpha_{\boldsymbol{r}_\ell+\boldsymbol{\delta}_z} \mathcal{S}^\beta_{\boldsymbol{r}_\ell+\boldsymbol{\delta}_z}$$
$$+ J^{ab} \sum_{\ell\in\triangledown} \sum_{j=1}^{3} \left(\mathcal{S}^x_{\boldsymbol{r}_\ell} \mathcal{S}^x_{\boldsymbol{r}_\ell+\boldsymbol{\delta}_j} + \mathcal{S}^y_{\boldsymbol{r}_\ell} \mathcal{S}^y_{\boldsymbol{r}_\ell+\boldsymbol{\delta}_j} + \Delta^{ab} \mathcal{S}^z_{\boldsymbol{r}_\ell} \mathcal{S}^z_{\boldsymbol{r}_\ell+\boldsymbol{\delta}_j} \right) + Q \sum_{\ell\in\triangledown} \sum_{j=1}^{3} \left(\mathcal{S}^y_{\boldsymbol{r}_\ell} \mathcal{S}^y_{\boldsymbol{r}_\ell+\boldsymbol{\delta}_j} \cos^2\phi_j + \mathcal{S}^x_{\boldsymbol{r}_\ell} \mathcal{S}^x_{\boldsymbol{r}_\ell+\boldsymbol{\delta}_j} \sin^2\phi_j \right), \quad (1)$$

where $\mathcal{S}^\alpha_{\boldsymbol{r}}$ is the αth component ($\alpha = x,y,z$) of the pseudospin-one operator at position $\boldsymbol{r}$, $\boldsymbol{r}_\ell$ is the position of site ℓ, $\boldsymbol{\delta}_z = (0,0,c)$, c is the interlayer spacing, $j = 1,2,3$ labels the nearest neighbor bonds as marked in Fig. 1, $\phi_j = 2\pi(j-1)/3$, $\boldsymbol{\delta}_j = (\sin\phi_j, \cos\phi_j, 0)a_g$ is the vector, of length a_g, connecting one sublattice to its three nearest neighbors in the plane, and $\sum_{\ell\in\triangledown}$ indicates that the sum runs over only the sublattice of triangles that point down in Fig. 1.

For large U, the magnitude of the antiferromagnetic exchange coupling between nearest neighbor clusters in the c direction J^c is much larger than the exchange coupling between nearest-neighbor clusters in the a-b plane J^{ab}, we

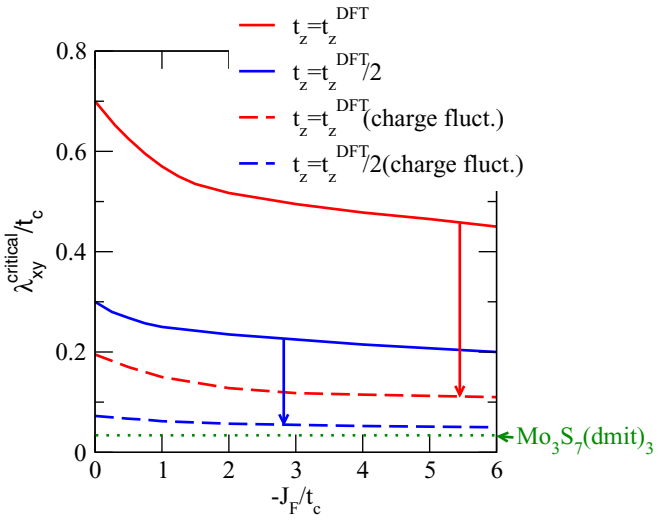

FIG. 3. Critical SMOC coupling for the transition from the Haldane to the D phase. At strong coupling, our effective spin exchange model consists of weakly coupled $S = 1$ antiferromagnetic chains in the presence of single-spin anisotropy, D^*. When the transverse SMOC $\lambda_{xy} > \lambda_{xy}^{\text{critical}}$ the D phase is stabilized whereas for $\lambda_{xy} < \lambda_{xy}^{\text{critical}}$ the Haldane phase occurs. The dependence of $\lambda_{xy}^{\text{critical}}$ with ferromagnetic intracluster exchange $-J_F$ is shown for model parameters: $\lambda_z = \lambda_{xy}/2$, $U = 10t_c$, and $t = 0.785t_c$ for two different hopping amplitudes along the chain; $t_z = t_z^{\text{DFT}} = 0.683t_c$ and $t_z = t_z^{\text{DFT}}/2$, where t_z^{DFT} is the value obtained from DFT calculations on the $Mo_3S_7(dmit)_3$ crystal. The full lines are obtained from the condition $D^*(\lambda_{xy}) \sim J^c$ assuming a Haldane spin gap opens in our spin model, while the dashed lines are obtained from $D^*(\lambda_{xy}) \sim 0.066J^c$ which includes renormalization effects due to charge fluctuations (not contained in our effective spin model) which strongly suppress the spin gap. The dotted horizontal line corresponds to the λ_{xy} obtained from DFT calculations on $Mo_3S_7(dmit)_3$ crystals. This figure shows that by reducing t_z and increasing $-J_F$, $Mo_3S_7(dmit)_3$ can be effectively driven close to the D phase. Varying the SMOC anisotropy also leads to significant changes in this curve; see in particular Eq. (B2).

conclude that the magnetic properties of two-thirds filled trinuclear coordination crystals can be effectively described by $S = 1$ XXZ chains with a local single-spin anisotropy D^* and anisotropic biquadratic terms $P_{\alpha\beta}$. We explore the effect of anisotropic SMOC, $\lambda_{xy} \neq \lambda_z$, finding that the largest anisotropic spin exchange couplings and single-spin anisotropies emerge when $\lambda_{xy}/\lambda_z < 1$, which is the relevant parameter regime for $Mo_3S_7(dmit)_3$.

For $Mo_3S_7(dmit)_3$ *ab initio* estimates of SMOC [13] indicate that $\lambda_{xy} \approx 0.042t_c$, and $\lambda_{xy} \approx \lambda_z/2$. This, suggests that single-spin anisotropies are smaller than the exchange coupling along the c direction, $D^* < J^c$, so that $Mo_3S_7(dmit)_3$ is in the Haldane phase rather than in the topologically trivial "D phase," i.e., the tensor product of the $j = 0$ singlets (where j is the z component of the total angular momentum) at each cluster, which is expected for $D^* > J^c$. In spite of the small SMOC values found in $Mo_3S_7(dmit)_3$ (see Fig. 3), the chemical flexibility of molecular crystals can significantly enhance λ_{xy} and λ_z, and suppress t_z. Together this could drive other related systems into the D phase and enhance anisotropies in the exchange interactions.

In Fig. 3 we show how the critical SMOC, $\lambda_{xy}^{\text{critical}}$, at which the transition from the Haldane to the D phase occurs, i.e., when $D^*(\lambda_{xy}) \sim J^c$, is strongly suppressed by reducing t_z and/or by a ferromagnetic intracluster exchange $-J_F$. Variations in the SMOC anisotropy (not shown) can also significantly vary D^* [see Appendix B and particularly, Eq. (B2)]. On the other hand, increasing U by, say, a factor of two does not change $\lambda_{xy}^{\text{critical}}$ since J^c is moderately influenced by U when $U \to \infty$. Intracluster charge fluctuations not captured by our spin model but present in the original Hubbard model are found to strongly suppress the spin gap [27]. For the microscopic parameters found from density functional theory (DFT) [13,16] for $Mo_3S_7(dmit)_3$ the transition line is given by $D^* \sim 0.066J^c$. The charge fluctuation effect suppresses $\lambda_{xy}^{\text{critical}}$ even further becoming comparable to the SMOC in $Mo_3S_7(dmit)_3$ crystals. Hence, even though SMOC is small in $Mo_3S_7(dmit)_3$ it may be possible to drive it from the Haldane to the D phase by modifying crystal parameters, in particular, by suppressing t_z. This may be achieved by applying negative uniaxial pressure along the c direction of the crystal which increases the interlayer distance. Alternatively, an expansion along the c direction can be achieved by applying uniaxial (positive) pressure on the a-b directions through the Poisson effect. However, this procedure can lead to changes in the in-plane arrangement of the molecules distorting the physics of the honeycomb lattice discussed here.

We analyze the possible magnetic anisotropies arising in the decorated honeycomb lattice of Fig. 1, which can be realized by isolating the a-b planes of trinuclear clusters. More specifically, we analyze the role played by the interplay of Coulomb repulsion, intracluster exchange, and SMOC in producing anisotropic exchange couplings. We study the role played by SMOC anisotropy, $\lambda_{xy} \neq \lambda_z$, which is generically the case in these systems and has not been considered previously. We find that the effective exchange couplings within the a-b planes are anisotropic *only* when *both* SMOC *and* intracluster exchange J_F are present. These magnetic anisotropies lead to a spin-one XXZ + 120° degree honeycomb quantum compass model with single spin anisotropy. In the limit of $J_F \to 0$, our effective spin exchange model reduces to the conventional isotropic $S = 1$ antiferromagnetic Heisenberg model on a honeycomb lattice.

We predict that under a sufficiently large external magnetic field, the Haldane phase can be destroyed giving way to a three-dimensional ordered magnet. This occurs at a critical magnetic field, $h_c \sim \Delta_s$, where Δ_s is the zero-field Haldane gap of the $S = 1$ chain.

The present paper is organized as follows. In Sec. II we introduce the minimal strongly correlated model for describing the electronic properties of isolated triangular molecules in the presence of SMOC. The physics of a single molecule described by this model is discussed in Appendix A. In Sec. III we analyze the electronic structure of two coupled trimers arranged as two nearest-neighbor molecules in the a-b plane and also as two nearest-neighbor molecules along the c direction. The energy level spectra of two coupled trimers is obtained exactly and compared to second-order perturbation theory. In Sec. IV the combination of the numerical

perturbative approach with an analytical canonical transformation (see also Appendix B), used to extract the exchange interactions between the nearest neighbor pseudospins, is detailed. In Sec. V, we discuss the qualitative phase diagram expected for the quasi-one-dimensional spin model arising from our approach. Finally, in Sec. VI, we conclude providing an outlook of our work.

II. MODEL OF ISOLATED TRIMERS IN THE PRESENCE OF SMOC

Here we consider crystals formed of triangular tri-nuclear molecules. In order to understand the effects of SMOC on the electronic and magnetic properties of these systems we first discuss the relevant model for isolated triangular clusters. The simplest strongly correlated model is a Hubbard model on a triangle in the presence of SMOC [16,28,29]:

$$H = H_0 + H_{\mathrm{SMOC}} + H_{U-J_F}. \tag{2}$$

In general all operators should also have a molecular label but this is suppressed throughout the current section as we deal only with a single complex.

The tight-binding part reads

$$H_0 = -t_c \sum_{\langle ij\rangle\sigma} (a^\dagger_{i\sigma} a_{j\sigma} + \mathrm{H.c.}), \tag{3}$$

where t_c is the hopping between the hybrid metal-ligand orbitals at nearest-neighbor sites in the cluster and $a^\dagger_{i\sigma}$ creates an electron at the ith Wannier orbital with spin σ.

The general SOC contribution is [12]

$$H_{\mathrm{SOC}} = \mathbf{K}\cdot\mathbf{S}, \tag{4}$$

where $\mathbf{S}$ is the electron spin and $\mathbf{K}$ is a pseudovector operator,

$$\mathbf{K} = \frac{\hbar}{4m^2c^2}[\mathbf{p}\times\nabla V(\mathbf{r})]. \tag{5}$$

We project onto a basis of one Wannier orbital per site of the model illustrated in Fig. 1. The two spin states of the Wannier orbital are a Kramers pair thus this projection removes all nontrivial effects of the atomic SOC. For example, in $Mo_3S_7(dmit)_3$ the Mo atoms are in a C_1 environment. Consider an atom with $\mathbf{L}\cdot\mathbf{S}$ atomic SOC in a C_1 environment with time-reversal symmetry. The most general coupling between two states is $\mathbf{B}^*\cdot\mathbf{S} + C^*\mathbb{1}$ (the most general 2×2 Hamiltonian). However, we require that these states remain degenerate to maintain time-reversal symmetry. Thus only the C^* term remains, providing a constant energy shift as the only effect of atomic SOC in the subspace of the Kramers pair. Note that the $\mathbf{B}^*$ term is an orbital Zeeman splitting term; if we had projected onto more Wannier orbitals, this term could be nonzero. It has been argued that this is relevant to some transition metal oxides [30,31] where this projection induces an effective anisotropy on the atomic SOC. Thus the only SOC term possible in our model is the direct coupling of the spin to currents running around the plane of the molecule (SMOC).

The SMOC contribution can be obtained by projecting the SOC operator of Eq. (4), using a multiatom potential $V(r)$ for the molecule [32] (instead of the conventional central potential of a single atom/ion used in transition metal oxides) into the molecular Wannier orbital basis [12,13]. Note that this does not mean that SMOC is just the linear superposition of atomic SOC since the expectation value of momentum of electrons in the molecule is, in general, very different from the expectation value of electrons orbiting a single atom. SMOC has a similar origin to atomic SOC, since it can be derived from a multiatomic potential describing the molecule, however, the orbital currents around the plane of the molecule are intrinsic to the molecular structure of multinuclear organometallic complexes and this results in the form of the interaction described below.

For C_3 symmetric molecules it can be shown [12] the SMOC is

$$\begin{aligned} H_{\mathrm{SMOC}} &= \lambda_{xy}(L_xS_x + L_yS_y) + \lambda_z L_z S_z \\ &= \lambda_{xy}\left(\frac{L^+S^- + L^-S^+}{2}\right) + \lambda_z L_z S_z, \end{aligned} \tag{6}$$

where L is the molecular-orbital angular momentum of electrons in the cluster, λ_{xy} describes the transverse SMOC, while λ_z describes the longitudinal contribution.

Finally, the Hubbard-Heisenberg term reads

$$H_{U-J_F} = U\sum_i n_{i\uparrow}n_{i\downarrow} + J_F\sum_{\langle ij\rangle}\left(\mathbf{S}_i\cdot\mathbf{S}_j - \frac{n_i n_j}{4}\right), \tag{7}$$

where U is the onsite Hubbard interaction, J_F is an intracluster exchange interaction, and $n_{i\sigma} = a^\dagger_{i\sigma}a_{i\sigma}$ the number operator. The *direct* exchange J_F between electrons at nearest-neighbor sites is generically nonzero and favors ferromagnetic tendencies, i.e., it is expected to be negative, $J_F < 0$. We will see below that, even if it is much smaller than the direct Coulomb interaction, J_F plays a crucial role in generating magnetic anisotropies. It plays a similar role as the Hunds coupling in transition metal oxides [4], which also generates magnetic exchange anisotropies between spins in the lattice.

The noninteracting part (3) can be readily diagonalized:

$$H_0 = \sum_{k\sigma}\epsilon_k b^\dagger_{k\sigma} b_{k\sigma}, \tag{8}$$

using Bloch operators,

$$b^\dagger_{k\sigma} = \frac{1}{\sqrt{3}}\sum_{j=1}^{3} e^{ik\phi(j-1)}a^\dagger_{j\sigma}, \tag{9}$$

with $\phi = 2\pi/3$. $k = 0, \pm 1$ correspond to the allowed $0, \pm\frac{2\pi}{3}$ momenta in the first Brillouin zone of the triangular cluster with energies $\epsilon_0 = -2t_c$ and $\epsilon_1 = \epsilon_{-1} = t_c$.

The SMOC contribution to H is most naturally described using "Condon-Shortley" states which are eigenstates of the z component of the angular momentum L_z of the cluster [12,33],

$$c^\dagger_{k\sigma} = \mathrm{sgn}^k(-k)\frac{1}{\sqrt{3}}\sum_{j=1}^{3} e^{ik\phi(j-1)}a^\dagger_{j\sigma}. \tag{10}$$

More explicitly we have

$$c^\dagger_{0,\sigma} = b^\dagger_{0\sigma}, \quad c^\dagger_{1\sigma} = -b^\dagger_{1,\sigma}, \quad c^\dagger_{-1\sigma} = b^\dagger_{-1,\sigma}. \tag{11}$$

Note that as Bloch's theorem applies to the cluster, the z component of angular momentum is defined up to $3n$ (in units of ϕ) with n an integer, i.e., Bloch states with momentum k' satisfying $k = k' \pm 3n$ are equivalent to the $k = 0, \pm 1$ states.

Hence, the tight-binding part of the Hamiltonian H_0 can be expressed either in terms of the Condon-Shortley or Bloch operators as

$$H_0 = -2t_c \sum_{\sigma,k=-1}^{1} \cos(\phi k) c^\dagger_{k\sigma} c_{k\sigma} = -2t_c \sum_{\sigma,k=-1}^{1} \cos(\phi k) b^\dagger_{k\sigma} b_{k\sigma}. \tag{12}$$

Similarly, from the expressions of the angular momentum in terms of the Bloch states,

$$L^+ = \sqrt{2}\sum_\sigma (b^\dagger_{0\sigma} b_{-1\sigma} - b^\dagger_{1\sigma} b_{0\sigma}), \quad L^- = \sqrt{2}\sum_\sigma (-b^\dagger_{0\sigma} b_{1\sigma} + b^\dagger_{-1\sigma} b_{0\sigma}), \quad L_z = \sum_{k\sigma} k b^\dagger_{k\sigma} b_{k\sigma}, \tag{13}$$

the SMOC contribution to the Hamiltonian of the isolated cluster reads

$$H_{\rm SMOC} = \frac{\lambda_{xy}}{\sqrt{2}}(b^\dagger_{0\downarrow} b_{-1\uparrow} - b^\dagger_{1\downarrow} b_{0\uparrow} - b^\dagger_{0\uparrow} b_{1\downarrow} + b^\dagger_{-1\uparrow} b_{0\downarrow}) + \frac{\lambda_z}{2}(b^\dagger_{1\uparrow} b_{1\uparrow} - b^\dagger_{1\downarrow} b_{1\downarrow} - b^\dagger_{-1\uparrow} b_{-1\uparrow} + b^\dagger_{-1\downarrow} b_{-1\downarrow}). \tag{14}$$

We may also express H in the site basis $|i\sigma\rangle$, using the transformation of Eq. (9) which leads to

$$\begin{aligned} H = & \sum_\sigma ((-t_c + \sigma\lambda_z B^*) a^\dagger_{1\sigma} a_{2\sigma} + (-t_c + \sigma\lambda_z B) a^\dagger_{1\sigma} a_{3\sigma} + (-t_c + \sigma\lambda_z B^*) a^\dagger_{2\sigma} a_{3\sigma} + \text{H.c.}) \\ & + \lambda_{xy}\sqrt{2}(A a^\dagger_{1\downarrow} a_{2\uparrow} + A^* a^\dagger_{1\downarrow} a_{3\uparrow} - A a^\dagger_{2\downarrow} a_{1\uparrow} + B^* a^\dagger_{2\downarrow} a_{3\uparrow} - A^* a^\dagger_{3\downarrow} a_{1\uparrow} + B a^\dagger_{3\downarrow} a_{2\uparrow}) + \text{H.c.} \\ & + U \sum_i n_{i\uparrow} n_{i\downarrow} + J_F \sum_{\langle ij\rangle} \left(\mathbf{S}_i \cdot \mathbf{S}_j - \frac{n_i n_j}{4}\right), \end{aligned} \tag{15}$$

with $A = \frac{(e^{i\phi}-1)}{6}$, $B = \frac{i}{3}\sin(\phi)$, and $\sigma = \pm 1$. It is evident from the above Hamiltonian that SMOC can be understood as a spin-dependent hopping between nearest-neighbor sites of the trimers.

Four-component relativistic *ab initio* calculations [13] for $Mo_3S_7(dmit)_3$ have found anisotropic SMOC: $\lambda_{xy} \approx \lambda_z/2 > 0$; cf. Table I. Below we will fix $t_c > 0$ as the unit of energy and explore different values of SMOC and different λ_{xy}/λ_z ratios. Note that the electronic properties of the model are invariant under the particle-hole transformation $a^\dagger_i \to h_i, a_i \to h^\dagger_i$, where $h^\dagger_i$ and h_i are hole operators together with the transformation $t_c \to -t_c$, $\lambda_{xy} \to -\lambda_{xy}$, $\lambda_z \to -\lambda_z$. The onsite Coulomb repulsion within each Wannier orbital U is comparable to or even larger than the bandwidth of the relevant $Mo_3S_7(dmit)_3$ bands crossing the Fermi energy. We will assume $U = 10t_c$ as a reasonable estimate. Since the $Mo_3S_7(dmit)_3$ crystal is at 2/3-filling there are $N = 4$ electrons per triangular cluster in the crystal. In order to fully characterize the electronic structure of two coupled clusters through perturbation theory techniques we have analyzed triangular clusters with $N = 3,4,5$ electrons and the parameters $t_c, \lambda_{xy}, \lambda_z > 0$, relevant to $Mo_3S_7(dmit)_3$ crystals. Through the particle-hole transformation we can also obtain the electronic structure of triangular clusters with $N = 1$ ($N = 2$) electrons from the $N = 5$ ($N = 4$) solutions by switching the sign of $\lambda_{xy}, \lambda_z, t_c$.

TABLE I. List of parameters entering our microscopic model for $Mo_3S_7(dmit)_3$. The exchange couplings of our derived effective spin exchange model (37) using the actual DFT parameters [13] obtained for the crystal are also tabulated. The exchange couplings are isotropic so α can be x, y, z. Parameters of the effective model that are smaller than 10^{-4} are not included. All energy units are in eV.

t_c	t	t_z	λ_{xy}	λ_z	J^{ab}	J^c
0.06	0.047	0.041	0.0025	0.005	0.0024	0.01296

Since $J_z = L_z + S_z$ is a conserved quantity, $[J_z, H] = 0$, it is convenient to use the (k,σ) representation instead of the site representation to classify the basis states according to their quantum number, $j = k + \sigma$. We have already expressed $H_0 + H_{\rm SMOC}$ in the (k,σ) basis through Eqs. (12)–(14). The Hubbard-Heisenberg contribution is expressed in the (k,σ) basis as

$$\begin{aligned} H_{U-J_F} = & \frac{1}{3}\sum_k (U - 2J_F) n_{k\uparrow} n_{k\downarrow} \\ & + \frac{1}{3}\sum_{k,k',k\neq k'} (U - J_F\cos((k-k')\phi) - J_F) n_{k\uparrow} n_{k'\downarrow} \\ & + \frac{1}{3}\sum_{k,k',q\neq 0} (U - J_F\cos((k'-k-q)\phi) \\ & - J_F\cos(q\phi)) b^\dagger_{k\uparrow} b^\dagger_{k'\downarrow} b_{k'-q\downarrow} b_{k+q\uparrow}. \end{aligned} \tag{16}$$

For the triangular clusters studied here $\frac{1}{3}\sum_{k,k',k\neq k'}(U - J_F\cos((k-k')\phi) - J_F) n_{k\uparrow} n_{k'\downarrow} = (U/3 - J_F/6)\sum_{k,k',k\neq k'} n_{k\uparrow} n_{k'\downarrow}$. Note that while for the Hubbard-Heisenberg model the effective Coulomb repulsion between electrons is different for electrons in different orbitals, in a pure Hubbard model ($J_F = 0$), all Coulomb interactions are equal to $U/3$. This has been shown to be important for finding spin exchange anisotropies in the context of transition metal oxides [5,34].

Hence, the full Hamiltonian can be explicitly expressed in the (k,σ) basis using the expressions for H_0, $H_{\rm SMOC}$, and H_{U-J_F} in Eqs. (12), (14), and (16), respectively.

In Appendix A we present results for the electronic structure of trimers with $N = 3,4,5$ electrons expressed in this basis. From this analysis, we conclude that isolated trimers with $N = 4$ electrons in the presence of SMOC effectively behave

as pseudospin-one localized moments. In Fig. 4 we show that under SMOC the lowest energy triplet splits into a nondegenerate singlet ($j = 0$) and a doublet ($j = \pm 1$), where j is the z component of total angular momentum. Higher energy excitations are doublets or nondegenerate under SMOC. Note that since we have an even number of electrons in the cluster, Kramers theorem does not apply and nondegenerate states are possible. Hence, SMOC induces a single-spin anisotropy at each cluster so that the effective spin model for $N = 4$ electrons in the mth $Mo_3S_7(dmit)_3$ molecule in the crystal reads

$$H_m^{\text{eff}} = D\left(S_{r_m}^z\right)^2. \tag{17}$$

As shown in Fig. 4 the overall energy level structure of the cluster, i.e., level splittings and degeneracies remain unaffected by anisotropies in SMOC, $\lambda_{xy} \neq \lambda_z$ and/or intracluster exchange $J_F \neq 0$. However, the absolute value of D is strongly enhanced when $\lambda_{xy}/\lambda_z < 1$ as shown in Fig. 5. This is directly relevant to $Mo_3S_7(dmit)_3$ crystals in which $\lambda_{xy}/\lambda_z \approx 1/2$.

III. TWO COUPLED TRIANGULAR CLUSTERS

We now consider two triangular coupled clusters. We analyze the electronic structure of two nearest neighbor triangular clusters as arranged in $Mo_3S_7(dmit)_3$ crystals and shown in Fig. 2. In Fig. 2(a) we show two nearest-neighbor clusters in the a-b plane, whereas in 2(b) we show two nearest-neighbor clusters along the c-direction. The molecules in the "dumbbell" configuration of Fig. 2(a) are related by inversion symmetry as in $Mo_3S_7(dmit)_3$. Molecules in the "tube" configuration of Fig. 2(b) are related by a rigid translation along the c-axis but no inversion symmetry is present. We first report exact results for the energy level structure. This gives key information about the type of spin exchange acting between the effective pseudospins localized at each trimer. These exact results are also used to benchmark perturbation theory calculations discussed in Sec. III B.

A. Electronic structure

Consider a model of two trimers, ℓ and m coupled by H_{kin}:

$$H = H_\ell + H_m + H_{\text{kin}}, \tag{18}$$

where H_ℓ is the Hubbard-Heisenberg model of an isolated trimer ℓ, in the presence of SMOC as introduced previously, Eq. (15) in Sec. II B. The hopping between two neighbor clusters is described through H_{kin}.

As shown in Fig. 2(a), in the coplanar dumbbell arrangement, there is only one hopping amplitude connecting the trimers, so H_{kin} reads

$$H_{\text{kin}}^{\text{dumbbell}} = -t \sum_\sigma (a_{\ell 1\sigma}^\dagger a_{m1\sigma} + a_{m1\sigma}^\dagger a_{\ell 1\sigma}), \tag{19}$$

which connects, say, site 1 of the ℓ cluster with site 1 of the m cluster. Here $a_{mi\sigma}^{(\dagger)}$ annihilates (creates) an electron with spin σ in the ith Wannier orbital on molecule m. The kinetic energy contains off-diagonal hopping matrix elements in the Bloch basis:

$$H_{\text{kin}}^{\text{dumbbell}} = -\frac{t}{3} \sum_{k_1,k_2,\sigma} \left(b_{\ell k_1\sigma}^\dagger b_{mk_2\sigma} + b_{mk_2\sigma}^\dagger b_{\ell k_1\sigma}\right), \tag{20}$$

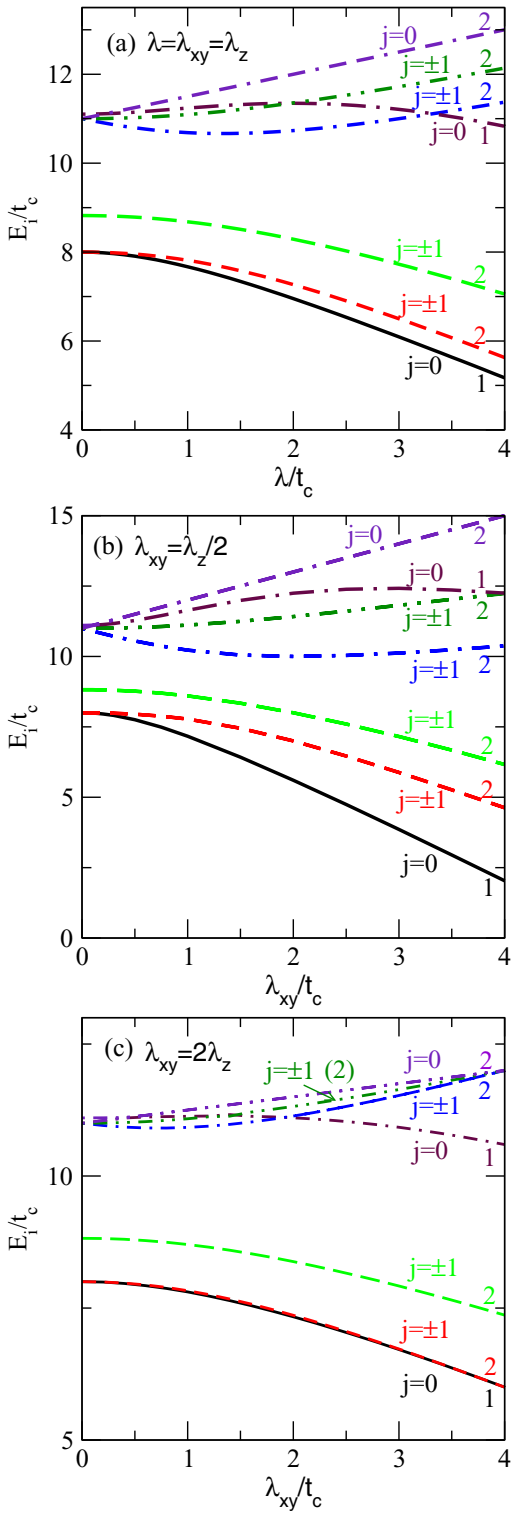

FIG. 4. Dependence of electronic structure of isolated triangular clusters on the strength and anisotropy of the SMOC. We plot the eigenvalues of Hamiltonian (15) with $N = 4$ electrons for $U = 10t_c$ and $J_F = 0$. We compare (a) the isotropic SMOC case, $\lambda = \lambda_{xy} = \lambda_z$, with anisotropic SMOC in (b) $\lambda_{xy} = \lambda_z/2$ and in (c) $\lambda_{xy} = 2\lambda_z$. The eigenstates are classified according to the z component of total angular momentum $j = k + \sigma$. The numbers denote energy level degeneracies. For $J_F \neq 0$ the electronic structure of the isolated cluster remains very similar, and in particular conserves the energy level degeneracies shown here.

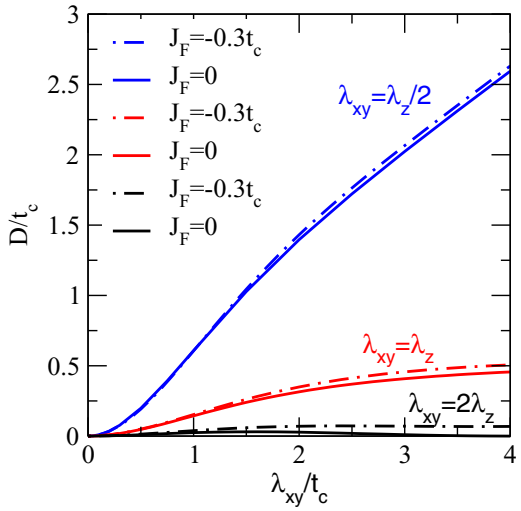

FIG. 5. Dependence of the single-spin anisotropy D of isolated triangular clusters on the strength and anisotropy of the SMOC. The energy difference between the lowest $j = \pm 1$ doublet and the ground state $j = 0$ singlet in Fig. 4, which defines D [cf. Eq. (17)], is plotted as a function of λ_{xy} for different λ_{xy}/λ_z ratios. A large enhancement of D is found when $\lambda_{xy} < \lambda_z$, which is relevant to $Mo_3S_7(dmit)_3$. Here, we have used $U = 10t_c$ and $J_F = 0, -0.3t_c$.

showing that the orbital momentum is not conserved in this case due to the breaking of trigonal symmetry.

In the tube arrangement, Fig. 2(b), the three vertices of the two clusters are connected by a hopping t_z, and $H_{\rm kin}$ reads

$$H_{\rm kin}^{\rm tube} = -t_z \sum_{i\sigma} (a^\dagger_{\ell i\sigma} a_{mi\sigma} + a^\dagger_{mi\sigma} a_{\ell i\sigma}). \qquad (21)$$

As the tubes respect the trigonal symmetry of the isolated trimers, the angular momentum about the C_3 axis is conserved. Hence, the kinetic energy between two trimers in the tube arrangement is diagonal when expressed in the Bloch basis:

$$H_{\rm kin}^{\rm tube} = -t_z \sum_{k,\sigma} (b^\dagger_{\ell k\sigma} b_{mk\sigma} + b^\dagger_{mk\sigma} b_{\ell k\sigma}), \qquad (22)$$

where $k = 0, \pm 1$, are the allowed momenta at each trimer of isolated trimers.

We have exactly diagonalized model (18) for two coupled triangular clusters in the presence of SMOC. We consider the case in which each cluster is filled with $N = 4$ electrons which is the relevant case for $Mo_3S_7(dmit)_3$ crystals. In Figs. 6(a) and 6(b) we show the dependence of the eigenenergies E_i on $\lambda = \lambda_{xy} = \lambda_z$ (isotropic SMOC) for $U = 10t_c$, $t = 0.785t_c$, and $J_F = 0$ in the dumbbell (a) and tube (b) arrangements. For $\lambda = 0$ we find that the eigenspectrum of the coupled trimers consists of a ground-state nondegenerate singlet, a triplet, and a pentuplet. This is the eigenspectrum expected for an *isotropic* antiferromagnetic exchange interaction between two localized $S = 1$ moments [29]. As λ is increased the energy levels are split partially removing $\lambda = 0$ degeneracies. The ground state of the coupled trimers is found to be nondegenerate for any value of λ.

In Figs. 6(c) and 6(d) we show the dependence of E_i on t for fixed SMOC, $\lambda = 0.25t$, and $\lambda = t$. In both cases the eigenenergies depend quadratically on t, $E_i \propto t^2$ up to large

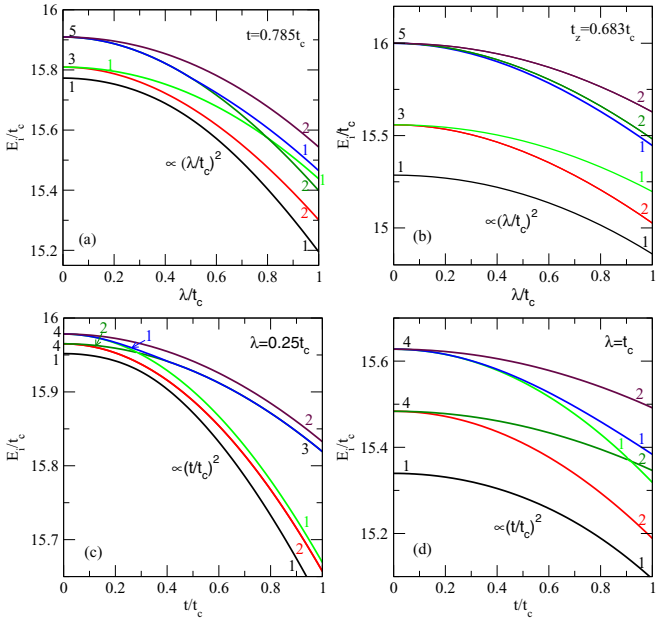

FIG. 6. Exact energy level spectra of two coupled trimers. The plots show exact eigenenergies of model (18) for $U = 10t_c$ and isotropic SMOC, $\lambda = \lambda_{xy} = \lambda_z$, and $J_F = 0$. The dependence of eigenstates E_i, with λ for $t = 0.785t_c$, are shown for the dumbbell (a) and tube arrangement (b). These plots show an $E_i \propto \lambda^2$ dependence. In (c) and (d) we fix λ and analyze the dependence of E_i on the hopping t in the dumbell configuration. A quadratic dependence, $E_i \propto t^2$, is found for both weak SMOC, $\lambda = 0.25t_c$ in (a), and strong SMOC, $\lambda = t_c$ in (d). The numbers denote the energy level degeneracies.

values of $t/t_c \sim 1$ indicating that second-order perturbation theory [$O(t^2)$] is reliable. Below, we will further analyze the accuracy of the $O(t^2)$ calculation for the model parameters that are relevant to $Mo_3S_7(dmit)_3$ crystals.

In order to understand these spectra, it is important to understand the symmetries of the models. This can be a little subtle when SMOC is included.

In the absence of SMOC the dumbbell model is D_{2h} symmetric as it also contains three mutually perpendicular twofold rotation axes [cf. Fig. 2(a)]. If two molecules, ℓ and m are related to one another by inversion symmetry then the pseudovectorial nature of angular momenta requires that the SMOC is equal on both molecules: $\lambda_{\ell,xy} = \lambda_{m,xy}$ and $\lambda_{\ell,z} = \lambda_{m,z}$. On the other hand if two molecules are related by a π rotation about, say, the z axis this yields $\lambda_{\ell,z} = \lambda_{m,z}$, but $\lambda_{\ell,xy} = -\lambda_{m,xy}$. This leads to significant changes in the effective interactions between the molecular spins, which we have discussed elsewhere [14,15]. Thus the case $\lambda_{\ell,xy} = \lambda_{m,xy}$ and $\lambda_{\ell,z} = \lambda_{m,z}$, which we consider here, lowers the symmetry to C_i (triclinic).

In the absence of SMOC the tube model is D_{3h} symmetric. This is lowered to C_{3v} in the presence of SMOC, which can be understood as follows. In our model $\lambda_{\ell,xy} = \lambda_{m,xy}$ and $\lambda_{\ell,z} = \lambda_{m,z}$. Under a mirror reflection with respect to a plane perpendicular to the z axis passing through the middle of the tube, i.e., a σ_h operation, there is a change in sign of the transverse SMOC contribution: $\lambda_{\ell,xy} = -\lambda_{m,xy}$, which would

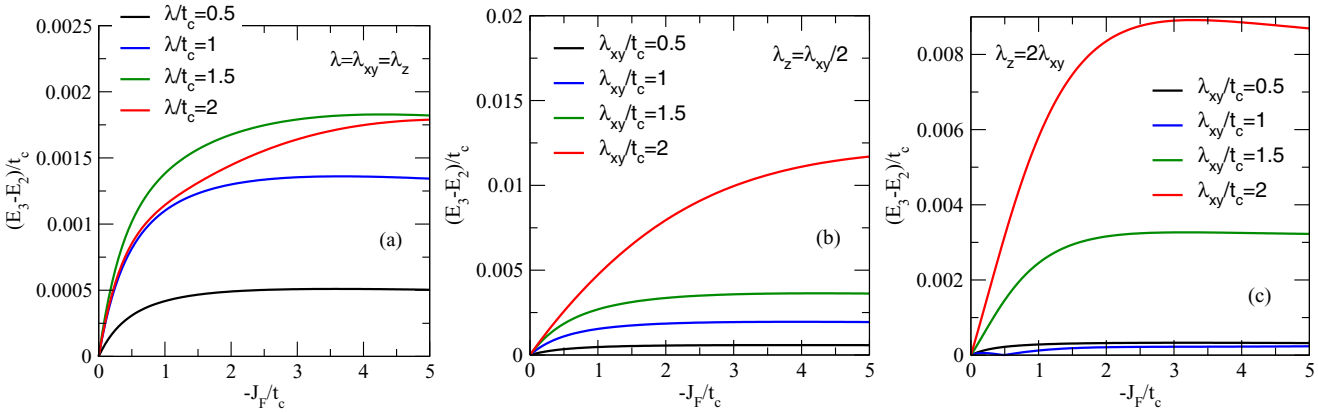

FIG. 7. Triclinic anisotropies induced by the Heisenberg intracluster exchange J_F, and SMOC λ_{xy},λ_z, for different ratios and strengths of SMOC. The energy difference between the exact third and second lowest energy levels for the dumbbell configuration is shown as a function of $-J_F$ (ferromagnetic direct exchange). We have fixed $U = 10t_c$, $t = 0.785t_c$ in all figures. In (a) we show results for the Hubbard-Heisenberg model with isotropic SMOC $\lambda = \lambda_{xy} = \lambda_z$, (b) $\lambda_z = \lambda_{xy}/2$, and in (c) $\lambda_z = 2\lambda_{xy}$. In contrast, in the case of the tube arrangement the energy splittings are zero: $E_3 - E_2 = 0$, for any value of J_F and λ_{xy}/λ_z ratio due to the trigonal (C_3) symmetry in that case.

be inconsistent with our model, except for $\lambda_{\ell,xy} = 0$. We find that our model is symmetric under C_3 rotations and only has three σ_v reflection planes. Hence, we conclude that the point group symmetry for the tube in the presence of SMOC is C_{3v}.

In both the dumbbell [Fig. 6(a)] and tube [Fig. 6(b)] configurations the $\lambda = 0$ triplet is split into a singlet and a doublet while the pentuplet is split into two doublets and a singlet. The energy levels are found to depend quadratically on λ: $E_i \propto \lambda^2$, indicating the absence of the linear DM antisymmetric exchange. In both cases this is expected on symmetry grounds. For the dumbbell this is straightforward, since there is an inversion center at the midpoint between the two triangular clusters [15,35]. For the tube the C_3 rotation symmetry implies that $\boldsymbol{D}^{\rm DM} \| z$ axis (Moriya's rule 5; Ref. [35]) and the σ_v reflection symmetry implies that $\boldsymbol{D}^{\rm DM} \| xy$ plane (Moriya's rule 3). Both conditions taken together lead to $\boldsymbol{D}^{\rm DM} = \boldsymbol{0}$, and there is no DM coupling between the two spins in the tube arrangement.

In $Mo_3S_7(dmit)_3$ the symmetry of the tube is lowered from C_{3v} to C_3 by small intermolecular interactions neglected in the current model [13]. This allows for a nonzero DM coupling parallel to the C_3 axis, which points along the crystallographic c axis [15].

The level degeneracies for both pairs of coupled clusters (Fig. 6) are those expected for an *isotropic* antiferromagnetic Heisenberg model with a trigonal single ion anisotropy described by Eq. (17), which we have seen arises for nonzero λ. This is expected for the tube, as in C_{3v} symmetry there are twofold degenerate states corresponding to the E irreducible representation.

However, the C_i symmetry of the dumbbell configuration admits only one-dimensional irreducible representations. Thus, one expects the level degeneracies associated with the trigonal symmetry to be fully lifted in the presence of SMOC. We will denote these level splittings as triclinic splittings. The absence of such triclinic splittings for $J_F = 0$ in the dumbbell arrangement therefore indicates a hidden symmetry in the model. This is broken for $J_F \neq 0$. To quantify the degree of hidden symmetry breaking we plot the difference in energy between the second and third eigenstates, $E_3 - E_2$ in Fig. 7. For $J_F = 0$ no level splitting is present for any λ_{xy}/λ_z ratio. However, a triclinic splitting arises as $-J_F$ is increased, saturating at sufficiently large $-J_F$. The largest splittings are found when SMOC is anisotropic, particularly when $\lambda_{xy}/\lambda_z > 1$.

Thus, it is apparent that hidden symmetry is related to the Coulomb matrix and is present in the absence of direct exchange interaction. For $J_F = 0$ the symmetric and antisymmetric spin exchange tensors are proportional, but this is lifted for $J_F \neq 0$. This hidden symmetry plays a similar role in controlling the anisotropy of effective spin models of transition metal oxides [36].

We stress that the C_3 rotation symmetry of the tube conformation forbids trigonal level splittings, even for $J_F \neq 0$. Consistent with this expectation, no triclinic level splittings are observed in our calculations for the tube configuration.

B. Second-order perturbation theory in the intercluster hopping

In order to derive a low-energy effective Hamiltonian for the two coupled clusters we now perform perturbation theory calculations to $O(t_{\rm conf}^2)$, where conf = dumbbell, tube and $t_{\rm dumbbell} = t$ and $t_{\rm tube} = t_z$. The effective Hamiltonian for two coupled clusters with N electrons in each cluster is given by

$$\begin{aligned} H_{\rm eff}^{(2),{\rm conf}} &= E_0(N, j_{\ell z})|N, j_{\ell z}\rangle\langle N, j_{\ell z}| \\ &\quad + E_0(N, j_{mz})|N, j_{mz}\rangle\langle N, j_{mz}| \\ &\quad + \sum_{|m_0\rangle} \frac{H_{\rm kin}^{\rm conf}|m_0\rangle\langle m_0|H_{\rm kin}^{\rm conf}}{2E_0(N,0) - \langle m_0|H_0 + H_U + H_{\rm SMOC}|m_0\rangle}, \end{aligned} \tag{23}$$

where $E_0(N, j_{iz})$, is the energy of the isolated trimer, i, with $j_{iz} = 0, \pm 1$ with N electrons ($N = 4$ in the case of interest here), with corresponding eigenstate $|N, j_{iz}\rangle$. In the expression above we are implicitly assuming that the ground state of

isolated uncoupled trimers is threefold degenerate even for nonzero SMOC. From a comparison to exact results and the canonical transformation, discussed below, we find that this approximation is very accurate for the parameter regime analyzed. The $\{|m_0\rangle\}$ are the complete set of virtual excitations in which an electron is transferred from one cluster to the other and may be written as

$$|m_0\rangle = |N-1,\gamma_\ell\rangle|N+1,\gamma_m\rangle = \sum_{\mu_\ell,\mu_m} A_{\gamma_\ell}(N-1,\mu_\ell)A_{\gamma_m}(N+1,\mu_m)|N-1,\mu_\ell\rangle|N+1,\mu_m\rangle, \tag{24}$$

where $A_{\gamma_i}(N\pm1,\mu_i) = \langle N\pm1,\mu_i|N\pm1,\gamma_i\rangle$, γ_i denotes the excitations, and μ_i runs over the Hilbert state configurations with $N\pm1$ electrons on trimer $i=\ell,m$.

Introducing these states in Eq. (23) we find for a given configuration of the coupled clusters,

$$\begin{aligned} H_{\rm eff}^{(2),\rm conf} &= E_0(N,j_{\ell z})|N,j_{\ell z}\rangle\langle N,j_{\ell z}| + E_0(N,j_{mz})|N,j_{mz}\rangle\langle N,j_{mz}| \\ &+ t_{\rm conf}^2 \sum_{\gamma_\ell,\gamma_m}\sum_{\sigma,\sigma'}\sum_{\mu_\ell,\nu_m,\mu'_\ell,\nu'_m} A_{\gamma_\ell}(N-1,\mu_\ell)A_{\gamma_m}(N+1,\nu_m)A^*_{\gamma_\ell}(N-1,\mu'_\ell)A^*_{\gamma_m}(N+1,\nu'_m) \\ &\times \frac{c^\dagger_{\ell1\sigma}c_{m1\sigma}|N-1,\mu_\ell\rangle|N+1,\nu_m\rangle\langle N+1,\nu'_m|\langle N-1,\mu'_\ell|c^\dagger_{m1\sigma'}c_{\ell1\sigma'}}{\Delta\epsilon(N-1,\gamma_\ell;N+1,\gamma_m)} \\ &+ t_{\rm conf}^2 \sum_{\gamma_\ell,\gamma_m}\sum_{\sigma,\sigma'}\sum_{\mu_m,\nu_\ell,\mu'_m,\nu'_\ell} A_{\gamma_\ell}(N+1,\nu_\ell)A_{\gamma_m}(N-1,\mu_m)A^*_{\gamma_m}(N-1,\mu'_m)A^*_{\gamma_\ell}(N+1,\nu'_\ell) \\ &\times \frac{c^\dagger_{m1\sigma}c_{\ell1\sigma}|N-1,\mu_m\rangle|N+1,\nu_\ell\rangle\langle N+1,\nu'_\ell|\langle N-1,\mu'_m|c^\dagger_{\ell1\sigma'}c_{m1\sigma'}}{\Delta\epsilon(N-1,\gamma_m;N+1,\gamma_\ell)}, \end{aligned} \tag{25}$$

where the excitation energies are $\Delta\epsilon(N-1,\gamma_\ell;N+1,\gamma_m) = 2E_0(N) - (E_{\gamma_\ell}(N-1) + E_{\gamma_m}(N+1))$.

It is important to test the reliability of the present second-order perturbative calculation for the values of the intercluster hopping amplitudes relevant to $Mo_3S_7(dmit)_3$ crystals. We have checked the accuracy of the second-order perturbation theory calculations by comparing the nine lowest energy eigenstates with the exact eigenspectrum in our previous work [14]. From Fig. 3 of [14] we concluded that the second-order $O(t^2)$ calculation is very accurate in the dumbbell arrangement with $U = 10t_c$, even for the large intermolecular hopping amplitude, $t = 0.785t_c$ relevant to $Mo_3S_7(dmit)_3$ crystals.

In the tube arrangement, comparable accuracies can only be achieved at larger U. The poorer accuracy at intermediate U in the tube configuration is due the stronger charge fluctuations in this configuration [27,28]. In the tube particles can be exchanged between the two clusters through $\sim t_z^2/t_c$ processes without paying energy cost $\sim U$ [15]. In contrast, in the dumbbell case, since particles can only be exchanged through the single hopping connecting the two vertices there is always an energy cost $\sim U$ inherent to the exchange process $\sim 4t^2/U$. In spite of this, at sufficiently large values of U we find that the second-order perturbation theory is sufficiently accurate for both the dumbbell and tube arrangements even for the large values of $t = 0.785t_c$ and $t_z = 0.683t_c$ extracted from DFT for $Mo_3S_7(dmit)_3$ [13,16].

IV. EFFECTIVE MAGNETIC SPIN EXCHANGE MODEL

In order to determine the analytical form of the pseudospin exchange Hamiltonian, we have performed a canonical transformation. Analytical expressions of the pseudospin model valid to $O(\lambda^2)$ and $O(t^2)$, are obtained assuming a t-J model for the triangular clusters, specified in Appendix B. By equating the matrix elements of the effective pseudospin exchange Hamiltonian obtained from the canonical transformation to the matrix elements of $H_{\rm eff}^{(2)}$ evaluated in the low-energy subspace $\{|j_\ell,j_m\rangle\}$, with $j_\ell,j_m = 0,\pm1$, we are able to extract the parameters entering the pseudospin exchange model.

A. Canonical transformation for a nearly degenerate low-energy subspace

Consider an arbitrary Hamiltonian, $H = H_0 + H_1$ where $H_0 = \sum_\nu P_\nu H P_\nu$, $H_1 = \sum_{\mu\neq\nu} P_\nu H P_\mu$, and P_ν is a projector onto the νth subspace. Now define $H(\varepsilon) = H_0 + \varepsilon H_1$. Let

$$\begin{aligned} \overline{H}(\varepsilon) &\equiv e^{-i\varepsilon S}H(\varepsilon)e^{i\varepsilon S} \\ &= H_0 + \varepsilon(H_1 + i[H_0,S]) \\ &\quad + \frac{\varepsilon^2}{2}(2i[H_1,S] - [[H_0,S],S]) + \cdots \end{aligned} \tag{26}$$

We choose S so that the linear term vanishes, i.e., such that $iH_1 = [H_0,S]$. This implies that

$$\begin{aligned} &P_\mu H P_\nu(1-\delta_{\mu\nu}) + iP_\mu H P_\mu(P_\mu S P_\nu) \\ &\quad - i(P_\mu S P_\nu)P_\nu H P_\nu = 0, \end{aligned} \tag{27}$$

because $P_\mu P_\nu = P_\mu\delta_{\mu\nu}$ and $\sum_\mu P_\mu = 1$. For $\mu = \nu$ this yields $P_\mu S P_\mu = \gamma P_\mu$ for $\gamma\in\mathbb{C}$. While, for $\mu\neq\nu$ we find

$$iP_\mu H P_\nu = P_\mu H P_\mu(P_\mu S P_\nu) - (P_\mu S P_\nu)P_\nu H P_\nu. \tag{28}$$

If we choose the projectors such that they project onto *strictly* degenerate subspaces then

$$P_\mu S P_\nu = \frac{iP_\mu H P_\nu}{\langle P_\mu H P_\mu\rangle - \langle P_\nu H P_\nu\rangle}. \tag{29}$$

Therefore, keeping only second-order $O(\varepsilon^2)$ terms, we find that

$$\begin{aligned}\overline{H} &\equiv \overline{H}(1) = H_0 + \frac{i}{2}[H_1, S] \\ &= \sum_{\mu} P_\mu H P_\mu - \frac{1}{2}\sum_{\mu\neq\nu}\sum_{\mu'\neq\nu} P_\mu H P_\nu H P_{\mu'} \\ &\quad\times\left(\frac{1}{\langle P_\nu H P_\nu\rangle - \langle P_{\mu'} H P_{\mu'}\rangle} + \frac{1}{\langle P_\nu H P_\nu\rangle - \langle P_\mu H P_\mu\rangle}\right).\end{aligned} \tag{30}$$

Finally, we find the effective low-energy Hamiltonian by projecting onto the low-energy subspace, henceforth denoted $\mathcal{L}$. Here it is convenient to associate all of the subspaces with the states chosen so that the low-energy subspace is diagonal, i.e., $P_\mu H P_\nu = 0$ if $\mu \neq \nu$ and both μ and $\nu \in \mathcal{L}$. (This is always possible provided we can solve the problem restricted purely to $\mathcal{L}$, as in elementary degenerate perturbation theory.) We then find that

$$\begin{aligned}H_{\text{eff}} &\equiv P_{\mathcal{L}}\overline{H}P_{\mathcal{L}} \\ &= \sum_{\mu\in\mathcal{L}} P_\mu H P_\mu - \frac{1}{2}\sum_{\mu,\mu'\in\mathcal{L}}\sum_{\nu\notin\mathcal{L}}\Big(\frac{P_\mu H P_\nu H P_{\mu'}}{\langle P_\nu H P_\nu\rangle - \langle P_{\mu'} H P_{\mu'}\rangle} \\ &\quad + \frac{P_\mu H P_\nu H P_{\mu'}}{\langle P_\nu H P_\nu\rangle - \langle P_\mu H P_\mu\rangle},\end{aligned} \tag{31}$$

where $P_{\mathcal{L}} = \sum_{\mu\in\mathcal{L}} P_\mu$. In the case that $\mathcal{L}$ is strictly degenerate this reduces to the standard result. In the case where there is a small spread of energies in $\mathcal{L}$ and these are treated as a single subspace, as in the derivation of the t-J model, a similar result holds but is approximate because the replacement of $P_\mu H P_\mu$ by its expectation value in Eq. (29) is no longer exact. We note that this is precisely the approximation made in Eq. (23) where we neglected the single-ion splitting of the ground-state triplet in the denominator.

The effective Hamiltonian derived from this canonical transformation describing the coupling between two isolated nearest-neighbor trimers, ℓ and m, in the tube arrangement of Fig. 2(b) is

$$\begin{aligned}H^c_{\ell m} &= D^c\left[\left(\mathcal{S}^z_{\boldsymbol{r}_\ell}\right)^2 + \left(\mathcal{S}^z_{\boldsymbol{r}_m}\right)^2\right] + \sum_{\alpha\beta} J^c_{\alpha\beta}\mathcal{S}^\alpha_{\boldsymbol{r}_\ell}\mathcal{S}^\beta_{\boldsymbol{r}_m} \\ &\quad + \sum_{\alpha\beta} P_{\alpha\beta}\mathcal{S}^\alpha_{\boldsymbol{r}_\ell}\mathcal{S}^\beta_{\boldsymbol{r}_\ell}\mathcal{S}^\alpha_{\boldsymbol{r}_m}\mathcal{S}^\beta_{\boldsymbol{r}_m},\end{aligned} \tag{32}$$

where $J^c_{\alpha\beta}$ is diagonal and $J^c_{xx} = J^c_{yy} \neq J^c_{zz}$, and the anisotropic biquadratic couplings, $P_{\alpha\beta} = P_{\beta\alpha}$, obey $P_{xx} = P_{yy} = P_{xy}$ and $P_{zx} = P_{zy} = (P_{zz} + P_{xx})/2$. Both numerically and analytically we find $P_{xx} \ll P_{zz}$, indeed we find numerically that P_{xx} is negligibly small and thus do not discuss it further below. $D^c = D + \Delta D^c$ is the single-spin anisotropy including corrections, ΔD^c, due to hopping processes between the clusters. The perturbative expressions for these parameters are given in Appendix B. Thus, one can recast the bilinear terms of $H^c_{\ell m}$ in the familiar XXZ form. Doing so, one finds that the Hamiltonian for a single chain is

$$\begin{aligned}H^c &= \sum_\ell D^c\left(\mathcal{S}^z_{\boldsymbol{r}_\ell}\right)^2 + \sum_{\ell\alpha\beta} P_{\alpha\beta}\mathcal{S}^\alpha_{\boldsymbol{r}_\ell}\mathcal{S}^\beta_{\boldsymbol{r}_\ell}\mathcal{S}^\alpha_{\boldsymbol{r}_\ell+\boldsymbol{\delta}_z}\mathcal{S}^\beta_{\boldsymbol{r}_\ell+\boldsymbol{\delta}_z} \\ &\quad + J^c\sum_\ell\left(\mathcal{S}^x_{\boldsymbol{r}_\ell}\mathcal{S}^x_{\boldsymbol{r}_\ell+\boldsymbol{\delta}_z} + \mathcal{S}^y_{\boldsymbol{r}_\ell}\mathcal{S}^y_{\boldsymbol{r}_\ell+\boldsymbol{\delta}_z} + \Delta^c\mathcal{S}^z_{\boldsymbol{r}_\ell}\mathcal{S}^z_{\boldsymbol{r}_\ell+\boldsymbol{\delta}_z}\right),\end{aligned} \tag{33}$$

where $J^c = J^c_{xx}$ and $\Delta^c = J^c_{zz}/J^c_{xx}$.

For two isolated nearest-neighbor trimers in the dumbbell arrangement with the t bond connecting the two sites labeled "1" [cf. Figs. 1 and 2(a)], the exchange Hamiltonian is

$$\begin{aligned}H^{ab}_1 &= D^{ab}\left[\left(\mathcal{S}^z_{\boldsymbol{r}_\ell}\right)^2 + \left(\mathcal{S}^z_{\boldsymbol{r}_\ell+\boldsymbol{\delta}_1}\right)^2\right] \\ &\quad + K_{\pm\pm}\left[\mathcal{S}^+_{\boldsymbol{r}_\ell}\mathcal{S}^+_{\boldsymbol{r}_\ell} + \mathcal{S}^+_{\boldsymbol{r}_\ell+\boldsymbol{\delta}_1}\mathcal{S}^+_{\boldsymbol{r}_\ell+\boldsymbol{\delta}_1} + \text{H.c.}\right] \\ &\quad + K_{z\pm}\left[\mathcal{S}^z_{\boldsymbol{r}_\ell}\mathcal{S}^x_{\boldsymbol{r}_\ell} + \mathcal{S}^z_{\boldsymbol{r}_\ell+\boldsymbol{\delta}_1}\mathcal{S}^x_{\boldsymbol{r}_\ell+\boldsymbol{\delta}_1} + \text{H.c.}\right] \\ &\quad + \sum_{\alpha\beta} J^{ab}_{\alpha\beta}\mathcal{S}^\alpha_{\boldsymbol{r}_\ell}\mathcal{S}^\beta_{\boldsymbol{r}_\ell+\boldsymbol{\delta}_1}.\end{aligned} \tag{34}$$

$D^{ab} = D + \Delta D^{ab}$ is the single-spin anisotropy including corrections ΔD^{ab}, due to hopping processes between the clusters and is plotted in Figs. 8 and 9. We find that ΔD^{ab} is very small so that $D^{ab} \sim D$.

To derive the effective Hamiltonian for the full crystal we now need to note that we have, so far, only considered the t bonds between Wannier orbitals labeled "1"; cf. Figs. 1 and 2, and Eq. (19). Rather than repeating the derivation for "2" and "3" bonds we can simply use the C_3 symmetry of the molecules and note that the $\boldsymbol{\mathcal{S}}_{\boldsymbol{r}_m}$ operators transform as vectors under rotation. Hence we can replace

$$\mathcal{S}^x_{\boldsymbol{r}_m} \to \mathcal{S}^x_{\boldsymbol{r}_m}\cos\phi_j - \mathcal{S}^y_{\boldsymbol{r}_m}\sin\phi_j, \tag{35a}$$

$$\mathcal{S}^y_{\boldsymbol{r}_m} \to \mathcal{S}^y_{\boldsymbol{r}_m}\cos\phi_j + \mathcal{S}^x_{\boldsymbol{r}_m}\sin\phi_j, \tag{35b}$$

in Eq. (34), where j labels the bond, as shown in Fig. 1.

First, one finds that the $K_{\pm\pm}$ and $K_{z\pm}$ terms vanish in the full crystal due to cancellation among the contributions from the three nearest-neighbor bonds. Transforming the other terms, one can rewrite that Hamiltonian as

$$\begin{aligned}H^{ab} &= \sum_\ell D^{ab}\left(\mathcal{S}^z_{\boldsymbol{r}_\ell}\right)^2 + J^{ab}\sum_{\ell\in\triangledown}\sum_{j=1}^{3}\left(\mathcal{S}^x_{\boldsymbol{r}_\ell}\mathcal{S}^x_{\boldsymbol{r}_\ell+\boldsymbol{\delta}_j} + \mathcal{S}^y_{\boldsymbol{r}_\ell}\mathcal{S}^y_{\boldsymbol{r}_\ell+\boldsymbol{\delta}_j} + \Delta^{ab}\mathcal{S}^z_{\boldsymbol{r}_\ell}\mathcal{S}^z_{\boldsymbol{r}_\ell+\boldsymbol{\delta}_j}\right) \\ &\quad + Q\sum_{\ell\in\triangledown}\sum_{j=1}^{3}\left(\mathcal{S}^y_{\boldsymbol{r}_\ell}\mathcal{S}^y_{\boldsymbol{r}_\ell+\boldsymbol{\delta}_j}\cos^2\phi_j + \mathcal{S}^x_{\boldsymbol{r}_\ell}\mathcal{S}^x_{\boldsymbol{r}_\ell+\boldsymbol{\delta}_j}\sin^2\phi_j\right) + J^{ab}_{xz}\sum_{\ell\in\triangledown}\sum_{j=1}^{3}\Big[\left(\mathcal{S}^x_{\boldsymbol{r}_\ell}\cos\phi_j - \mathcal{S}^y_{\boldsymbol{r}_\ell}\sin\phi_j\right)\mathcal{S}^z_{\boldsymbol{r}_\ell+\boldsymbol{\delta}_j} \\ &\quad + \mathcal{S}^z_{\boldsymbol{r}_\ell}\left(\mathcal{S}^x_{\boldsymbol{r}_\ell+\boldsymbol{\delta}_j}\cos\phi_j - \mathcal{S}^y_{\boldsymbol{r}_\ell+\boldsymbol{\delta}_j}\sin\phi_j\right)\Big],\end{aligned} \tag{36}$$

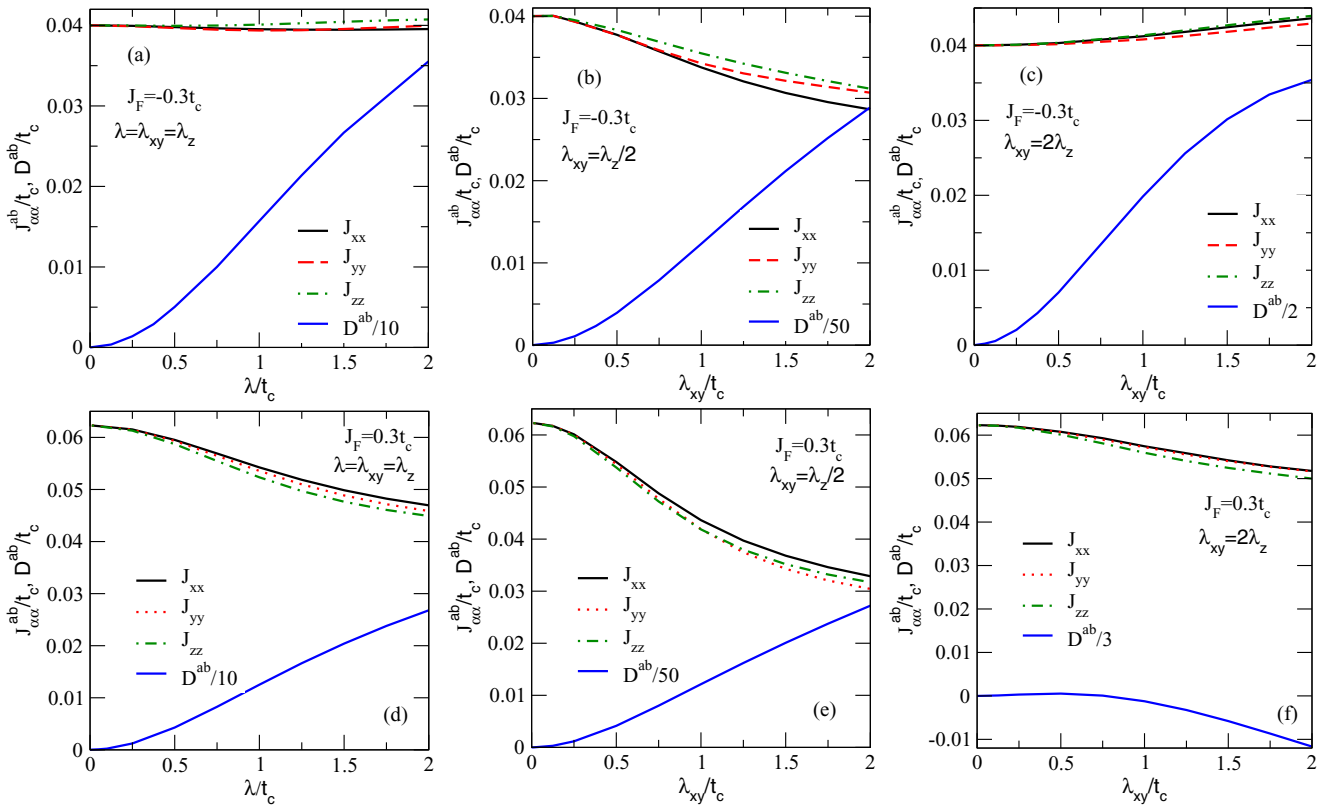

FIG. 8. Anisotropic exchange couplings and single-spin anisotropy in the a-b plane of trinuclear complexes. The dependence of the parameters entering model (34) on SMOC are shown for $U = 10t_c$. The hopping between the trimers is $t = 0.785t_c$. In the upper row panels we show the dependence on SMOC of the exchange couplings $J_{\alpha\alpha}$, and the single-spin anisotropy $D^{ab} = D + \Delta D^{ab}$ for different λ_{xy}/λ_z ratios in the presence of an intracluster ferromagnetic coupling, $J_F = -0.3t_c$: (a) $\lambda_{xy}/\lambda_z = 1$, (b) $\lambda_{xy}/\lambda_z = 1/2$, and (c) $\lambda_{xy}/\lambda_z = 2$. In the lower row panels [(d)–(f)] we show the same cases but with an intracluster antiferromagnetic exchange: $J_F = 0.3t_c$. The only nonzero off-diagonal exchange coupling, J^{ab}_{xz}, is at most $\sim -4.4 \times 10^{-4}$; too small to be appreciable in the scale of the figure.

where $J^{ab} = (J^{ab}_{xx} + J^{ab}_{yy})/2$, $\Delta^{ab} = J^{ab}_{zz}/J^{ab}$, and $Q = (J^{ab}_{xx} - J^{ab}_{yy})/2$. The perturbative expressions for these parameters are given in Appendix B. Thus, we see that the second term (proportional to J^{ab}) is simply the XXZ model and the third term (proportional to Q) is the honeycomb 120° compass model [3].

Finally, combining the results obtained above we obtain the full effective spin exchange model for the crystal, which reads

$$
\begin{aligned}
H_{\rm eff} = {} & D^* \sum_{\ell} \left(\mathcal{S}^z_{\boldsymbol{r}_\ell}\right)^2 + J^c \sum_{\ell} \left(\mathcal{S}^x_{\boldsymbol{r}_\ell}\mathcal{S}^x_{\boldsymbol{r}_\ell+\boldsymbol{\delta}_z} + \mathcal{S}^y_{\boldsymbol{r}_\ell}\mathcal{S}^y_{\boldsymbol{r}_\ell+\boldsymbol{\delta}_z} + \Delta^c \mathcal{S}^z_{\boldsymbol{r}_\ell}\mathcal{S}^z_{\boldsymbol{r}_\ell+\boldsymbol{\delta}_z}\right) + \sum_{\ell\alpha\beta} P_{\alpha\beta}\mathcal{S}^\alpha_{\boldsymbol{r}_\ell}\mathcal{S}^\beta_{\boldsymbol{r}_\ell}\mathcal{S}^\alpha_{\boldsymbol{r}_\ell+\boldsymbol{\delta}_z}\mathcal{S}^\beta_{\boldsymbol{r}_\ell+\boldsymbol{\delta}_z} \\
& + J^{ab} \sum_{\ell\in\triangledown}\sum_{j=1}^{3} \left(\mathcal{S}^x_{\boldsymbol{r}_\ell}\mathcal{S}^x_{\boldsymbol{r}_\ell+\boldsymbol{\delta}_j} + \mathcal{S}^y_{\boldsymbol{r}_\ell}\mathcal{S}^y_{\boldsymbol{r}_\ell+\boldsymbol{\delta}_j} + \Delta^{ab}\mathcal{S}^z_{\boldsymbol{r}_\ell}\mathcal{S}^z_{\boldsymbol{r}_\ell+\boldsymbol{\delta}_j}\right) + Q \sum_{\ell\in\triangledown}\sum_{j=1}^{3} \left(\mathcal{S}^y_{\boldsymbol{r}_\ell}\mathcal{S}^y_{\boldsymbol{r}_\ell+\boldsymbol{\delta}_j}\cos^2\phi_j + \mathcal{S}^x_{\boldsymbol{r}_\ell}\mathcal{S}^x_{\boldsymbol{r}_\ell+\boldsymbol{\delta}_j}\sin^2\phi_j\right) \\
& + J^{ab}_{xz} \sum_{\ell\in\triangledown}\sum_{j=1}^{3} \left[\left(\mathcal{S}^x_{\boldsymbol{r}_\ell}\cos\phi_j - \mathcal{S}^y_{\boldsymbol{r}_\ell}\sin\phi_j\right)\mathcal{S}^z_{\boldsymbol{r}_\ell+\boldsymbol{\delta}_j} + \mathcal{S}^z_{\boldsymbol{r}_\ell}\left(\mathcal{S}^x_{\boldsymbol{r}_\ell+\boldsymbol{\delta}_j}\cos\phi_j - \mathcal{S}^y_{\boldsymbol{r}_\ell+\boldsymbol{\delta}_j}\sin\phi_j\right)\right], \qquad (37)
\end{aligned}
$$

where $D^* = D + \Delta D^c + \Delta D^{ab}$. This expression neglects "three molecule" terms analogous to the "three site" terms neglected in the usual formulation of the t-J model [37,38]. We will see below that J^{ab}_{xz} is extremely small. On neglecting this term one finds that the effective Hamiltonian is given by Eq. (1).

The parameters governing the spin exchange between molecules ℓ and m in our spin exchange Hamiltonian $H_{\rm eff}$ are obtained by comparing the canonical transformation with our numerical second-order perturbation theory,

$$
\begin{aligned}
\langle j_\ell, j_m | H^{ab}_{lm} | j_\ell, j_m \rangle &= \langle j_\ell, j_m | H^{(2),\rm dumbbell}_{\rm eff} | j_\ell, j_m \rangle, \\
\langle j_\ell, j_m | H^{c}_{lm} | j_\ell, j_m \rangle &= \langle j_\ell, j_m | H^{(2),\rm tube}_{\rm eff} | j_\ell, j_m \rangle, \qquad (38)
\end{aligned}
$$

recall $H^{(2),\rm conf}_{\rm eff}$ is defined in Eq. (25). The above equations are solved for a given set of parameters: U, J_F, t_c, t, t_z, λ_{xy}, and λ_z entering our original microscopic model (2).

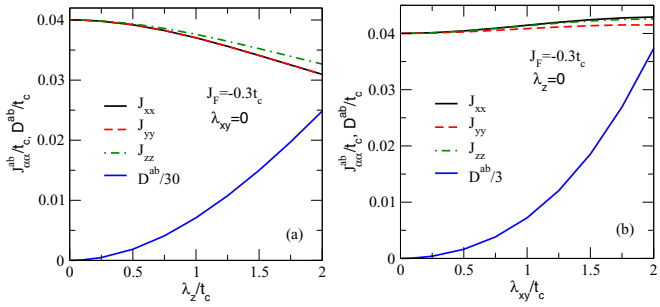

FIG. 9. Anisotropic exchange couplings in the a-b plane of trinuclear complexes in the limit of extreme SMOC anisotropies. The dependence on SMOC of the parameters entering model (34) are shown for $U = 10t_c$ and $J_F = -0.3t_c$. The hopping between the trimers is $t = 0.785t_c$. We compare different ratios of the SMOC: (a) $\lambda_{xy} = 0$ and (b) $\lambda_z = 0$.

B. Anisotropic exchange in the a-b plane

We have explored anisotropies arising in the exchange couplings of the effective exchange model, Eq. (34), for the two clusters coupled as in Fig. 2(a). Since the non-pseudospin-conserving $K_{\alpha\beta}$ terms exactly cancel in the crystal they will not be discussed any further. We find that when $J_F = 0$ the exchange coupling tensor is diagonal and isotropic, $J^{ab}_{\alpha\beta} = J^{ab}\delta_{\alpha\beta}$. This is consistent with our previous results [see Fig. 4(a) of Ref. [14]] and the lack of triclinic splittings observed in the energy level spectrum for two clusters in the dumbbell configuration shown in Fig. 7.

As shown in Fig. 8 anisotropic exchange couplings $J^{ab}_{xx} \neq J^{ab}_{yy} \neq J^{ab}_{zz}$ arise when $J_F \neq 0$, which are consistent with the triclinic splittings found in the exact level spectrum of Fig. 7. Also we find off-diagonal exchange couplings: $J^{ab}_{xz} \neq 0$ to all orders of SMOC consistent with the analytical expression for J^{ab}_{xz} derived in our previous work [14] valid to $O(\lambda^2_{xy},\lambda^2_z)$. However, we typically find small values of $J^{ab}_{xz} \sim -0.00044t_c$ ($\lambda_{xy} = \lambda_z/2$) and $J^{ab}_{xz} \sim -0.0003t_c$ ($\lambda_{xy} = \lambda_z$) and so this parameter is not displayed in Fig. 8. Therefore, to an excellent approximation, the in-plane Hamiltonian is an XXZ + 120° honeycomb model with single ion anisotropy.

Comparing the results shown in Fig. 8 for different λ_{xy}/λ_z ratios, we observe that the anisotropies in the exchange couplings are enhanced for $\lambda_{xy}/\lambda_z \neq 1$. In fact, larger anisotropies are found to occur for $\lambda_{xy} = \lambda_z/2$, which is the parameter regime relevant to $Mo_3S_7(dmit)_3$ crystals [13]. Also note from Fig. 8 the strong dependence of the magnitude of D^{ab} on the SMOC anisotropy. The single-spin anisotropy increases rapidly with SMOC, becoming equal to the exchange couplings, $D^{ab} \sim J^{ab}$ at $\lambda \approx 0.45t_c$ ($\lambda = \lambda_{xy} = \lambda_z$), at $\lambda_{xy} \approx 0.22t_c$ ($\lambda_{xy} = \lambda_z/2$), and at $\lambda_{xy} \approx 1.045t_c$ ($\lambda_{xy} = 2\lambda_z$). At sufficiently large $D^{ab} \gtrsim J^{ab}$ we expect the D phase, i.e., a tensor product of $j = 0$ states located at each cluster of the crystal. Hence, a D phase is favored by anisotropic SMOC with $\lambda_{xy} < \lambda_z$.

In Fig. 8 we also show results for an antiferromagnetic exchange coupling inside the cluster, $J_F > 0$. This could arise in, say, $Mo_3S_7(dmit)_3$ due to superexchange via the sulfur atoms in the core. We find similar spin exchange anisotropies for both ferromagnetic and antiferromagnetic J_F. In the antiferromagnetic case we find that D^{ab} becomes negative for sufficiently large SMOC and $\lambda_{xy} = 2\lambda_z$, consistent with our perturbative results for the t-J model [cf. Eqs. (B2), (B4a), and (B6a)]. This signifies a switch of the ground state of the isolated cluster from the $j = 0$ singlet to the $j = \pm 1$ doublet. In contrast, in the ferromagnetic cases, $J_F < 0$, we have explored a large parameter set and we always find $D^{ab} > 0$.

In order to understand the effect of exchange couplings with SMOC anisotropy, we show in Fig. 9 exchange couplings $J^{ab}_{\alpha\alpha}$ and D^{ab} in two extreme cases: $\lambda_{xy} = 0$ and $\lambda_z = 0$ with $J_F = -0.3t_c$. The $J^{ab}_{\alpha\alpha}$ are suppressed (enhanced) with SMOC for $\lambda_{xy} = 0$ ($\lambda_z = 0$), consistent with the results shown in Fig. 8. Only when λ_{xy} is turned on does one find that the transverse couplings become different, i.e., $J_{xx} \neq J_{yy}$. Furthermore, the single-spin anisotropy is much more strongly enhanced by λ_{xy} than by λ_z (by more than an order of magnitude), consistent with the analytical expressions [see Eqs. (B2), (B4a), and (B6a)].

C. Anisotropies in the exchange interactions along the c direction

The exchange couplings between two neighboring clusters in the c direction are shown in Fig. 10. We find a diagonal exchange tensor: $J^c_{\alpha\beta} = J^c_{\alpha\alpha}\delta_{\alpha\beta}$, with $J^c_{xx} = J^c_{yy} \neq J^c_{zz}$ for any $J_F \neq 0$ and λ_{xy}/λ_z ratio. The higher symmetry than for a pair of molecules in the a-b plane is due to the C_3 rotational symmetry of the tube dimer, as discussed above.

The largest anisotropies with $J^c_{xx} = J^c_{yy} > J^c_{zz}$ are seen in the case of anisotropic SMOC with $\lambda_{xy} = \lambda_z/2$ as shown in Fig. 10(b). The only non-negligible biquadratic exchange terms, $P_{zz} > P_{zx}$, increase rapidly with λ_{xy} starting to saturate around $\lambda/t_c \sim 1 - 1.5$. The single-spin anisotropy equals the exchange coupling, $D^c = J^c$, at $\lambda_{xy} = 0.65t_c$ for $\lambda_{xy}/\lambda_z = 1/2$ and at $\lambda_{xy} = 1.457t_c$ for $\lambda_{xy}/\lambda_z = 1$, while for $\lambda_{xy}/\lambda_z = 2$ there is no critical λ_{xy} at which $D^c \sim J^c$ within the parameter range explored. Hence, anisotropic SMOC with $\lambda_{xy} < \lambda_z$ again favors the D phase as in the dumbbell arrangement.

Finally, in Fig. 11 we compare the dependence of the exchange couplings on J_F for $\lambda_{xy} = \lambda_z = 1$. The couplings in the a-b plane, $J^{ab}_{\alpha\alpha}$ are suppressed and become gradually anisotropic, $J^{ab}_{xx} \neq J^{ab}_{yy} \neq J^{ab}_{zz}$, as J_F increases. This is in contrast to the exchange couplings in the c direction which do not display larger anisotropies but rather $J^c_{xx} = J^c_{yy} \neq J^c_{zz}$ for any J_F.

V. DISCUSSION OF PROPERTIES OF THE QUASI-ONE-DIMENSIONAL PSEUDOSPIN-ONE MODEL

Our analysis shows that the magnetic properties of layered decorated honeycomb lattice model at strong coupling, $U \gg t_c,t,t_z,\lambda_{xy},\lambda_z$, are captured by model (37) with the exchange couplings obtained from our combined approach described above. On comparing J^{ab} in Fig. 8 with J^c in Fig. 10 we find that $J^c \sim 5J^{ab}$ for $U = 10t_c$. This is related to the fact that two clusters in the tube arrangement are connected by three hoppings so that they can exchange electrons without paying an energy cost [14,15] $\sim U$. This mechanism is generic to decorated lattices and not specific to the model considered here [10]. In contrast, neighboring clusters in the dumbbell

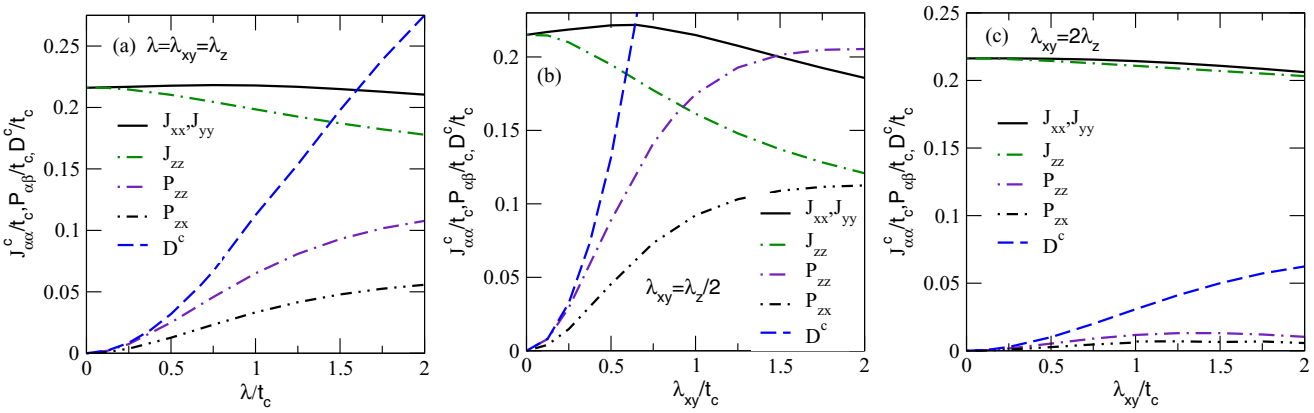

FIG. 10. Anisotropic exchange couplings in the c direction of trinuclear complexes. The dependence of the parameters entering model (34) on SMOC are shown for $U = 10t_c$ and $J_F = -0.3t_c$. The hopping between the trimers is $t_z = 0.683t_c$. We compare different SMOC anisotropies (a) $\lambda_{xy}/\lambda_z = 1$, (b) $\lambda_{xy}/\lambda_z = 1/2$, and (c) $\lambda_{xy}/\lambda_z = 2$. Note the large enhancement of the single-spin anisotropy, $D^c = D + \Delta D^c$, for anisotropic SMOC becoming the largest for $\lambda_{xy} < \lambda_z$. For $\lambda_{xy} = \lambda_z/2$, relevant to $Mo_3S_7(dmit)_3$ crystals [13], we have that $D^c \sim J^c_{xx} = J^c_{yy}$ at about $\lambda_{xy} = 0.65t_c$.

arrangement pay energy U, since they can only exchange particles through a single hopping connecting them. Hence, J^{ab} is strongly suppressed by U in contrast to J^c, leading to an increase of the J^c/J^{ab} ratio. Hence, at large U the system becomes quasi-one-dimensional consisting on a set of weakly coupled pseudo-spin-one antiferromagnetic chains.

An isotropic version of the model (33), i.e., $J^c_{\alpha\beta} = J^c\delta_{\alpha\beta}$ $P_{\alpha\beta} = P\delta_{\alpha\beta}$ and $D^c = 0$ is just the bilinear-biquadratic model: $H = J^c\sum_\ell \boldsymbol{\mathcal{S}}_{\boldsymbol{r}_\ell}\cdot\boldsymbol{\mathcal{S}}_{\boldsymbol{r}_\ell+\boldsymbol{\delta}_z} + P\sum_\ell(\boldsymbol{\mathcal{S}}_{\boldsymbol{r}_\ell}\cdot\boldsymbol{\mathcal{S}}_{\boldsymbol{r}_\ell+\boldsymbol{\delta}_z})^2$, which becomes the Affleck-Kennedy-Lieb-Tasaki (AKLT) model for $P/J^c = 1/3$. The AKLT model can be solved exactly and has the valence bond solid ground state and is in the Haldane phase [39].

We finally note that the next-nearest-neighbor exchange couplings between clusters in the c direction can be neglected since recent estimates [14] suggest that they are about 20 times smaller than the nearest-neighbor exchange coupling. This is because the small parameter in the perturbation theory is $t_z/3$ so fourth-order terms (such as next-nearest-neighbor exchange couplings) must be at least an order of magnitude smaller than second-order terms (such as nearest-neighbor exchange coupling).

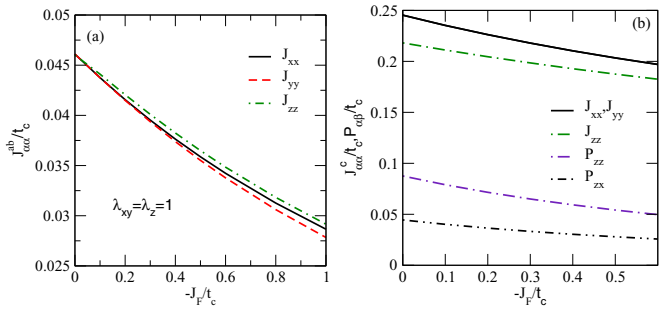

FIG. 11. Effect of the intracluster exchange J_F on the exchange couplings between trimers. In (a) we show the dependence of the exchange couplings in the a-b plane J^{ab} on $-J_F$ while in (b) we show the dependence of exchange couplings in the c direction J^c on $-J_F$. We have used $U = 10t_c$, $t = 0.785$, $t_z = 0.683$, and $\lambda_{xy} = \lambda_z = 1$.

A. One-dimensional antiferromagnetic $S = 1$ Heisenberg chains

When no interchain coupling is present, $J^{ab} = 0$ and $D^* < J^c$, the system consists on a set of uncoupled one-dimensional $S = 1$ antiferromagnetic chains that are in the Haldane phase. The Haldane phase is characterized by exponentially decaying spin correlations associated with [40] the Haldane spin gap $\Delta_s = 0.4107(3)J^c$ to the lowest triplet state and string order. It is a symmetry-protected topological phase with nonlocal string order and fractionalized edge states [41–43]. Topological protection can arise from either (i) the dihedral group of π rotations around the x and y axis, (ii) time-reversal symmetry, or (iii) reflection through a plane perpendicular to the chain (or bond-center inversion symmetry, which is equivalent in one dimension) [44]. In the underlying fermionic model, charge fluctuations imply that topological protection can only come from reflection symmetry with respect to a plane perpendicular to the c axis at the midpoint of a bond [27].

On the other hand, when $D^* \gg J^c$, the ground state is adiabatically connected to a trivial state consisting on the tensor product of the $\mathcal{S}^z_{\boldsymbol{r}_\ell} = 0$ at each cluster. The lowest energy excitations of the D phase which reside in the $\mathcal{S}^z_{\boldsymbol{r}_\ell} = \pm 1$ sector, are gapped and consist of pairs of excitons and antiexcitons which can be bound. Numerical studies [45–48] have established that in the pure spin model the quantum critical point separating the D phase and Haldane phase occurs at $D^*/J^c \sim 0.96 - 0.971$. It has been found that in a pure spin model such as the one discussed here, a quantum phase transition between the Haldane phase and the topologically trivial D phase is signaled by the change in sign of an inversion-symmetry-based order parameter [47] which is a nonlocal topological order parameter. Hence, a transition from a Haldane phase to a D phase occurs when increasing SMOC until $D^* \sim J^c$.

From our analysis of Fig. 10(b), which is the relevant SMOC ratio to $Mo_3S_7(dmit)_3$, (assuming $J_F = -0.3t_c$), we predict a transition from the Haldane to the D phase at $\lambda_{xy} \sim 0.65t_c$. *Ab initio* estimates of SMOC [13] in $Mo_3S_7(dmit)_3$ find that $\lambda_{xy} = \lambda_z/2 = 0.042t_c$, which would naively mean that the single-spin anisotropy is too small, $D^* \ll J^c$, to induce a D

phase in the crystal. By moving to suitable materials containing heavier elements [12], SMOC can be increased by, at most, a factor of 4–5 leading to $\lambda_{xy} \approx 0.2t_c \ll \lambda_{xy}^{\text{critical}}$ which means that the system is still in the Haldane phase. However, the critical λ_{xy} for the transition can be reduced by suppressing t_z and increasing $-J_F$ as shown in Fig. 3. Also in the underlying fermionic model (neglecting SMOC), the Haldane gap is suppressed by more than an order of magnitude by charge fluctuations [27]. More specifically, charge fluctuations renormalize the critical condition $D^* \sim J^c$ to $D^* \sim 0.066J^c$ for the parameters relevant to $Mo_3S_7(dmit)_3$. This leads to a smaller $\lambda_{xy}^{\text{critical}}$ as shown in Fig. 3. The above discussion indicates that a series of materials related to $Mo_3S_7(dmit)_3$ with slight variations in model parameters could easily effectively span the phase Haldane–to–D-phase transition. Furthermore, a material on the D-phase side of the transition could be driven into the Haldane phase by uniaxial pressure along the c axis. In particular, our results above suggest that the critical ratio D^*/J^c could be exceeded by moving to suitable materials containing heavier elements [12]. Furthermore, one expects that the interlayer hopping t_z will be extremely sensitive to chemical details. As $J^c \sim t_z^2$ structures with increased interlayer separation will strongly favor the D phase.

B. Effect of the interchain couplings

When the quantum pseudospin-one chains are coupled through a sufficiently strong interchain coupling J^{ab}, the Haldane phase becomes unstable to 3D magnetic order. In previous numerical studies of weakly coupled $S = 1$ antiferromagnetic Heisenberg chains (with $D^* = 0$), it was estimated [49] that the critical value for the transition from the Haldane to the ordered 3D magnet occurs around $J^{ab}/J^c \geqslant (0.08 - 0.11)z \sim 0.3$, where the coordination number $z = 3$ for the honeycomb lattice. Since we find that $J^{ab}/J^c \lesssim 0.2$, we expect that the ground state of our model is in the Haldane phase when $D^* = 0$. This critical ratio, J^{ab}/J^c, for the onset of 3D magnetic order is suppressed by D^* as shown [50] by mean-field treatments of the interchain coupling J^{ab}.

C. Effect of an external magnetic field

An external magnetic field suppresses the 1D quantum fluctuations and the Haldane gap Δ_s closes [51] at $h_c \sim \Delta_s$, when a transition to a 3D ordered magnet occurs. A quantum critical region with a V shape emerges around h_c in the temperature versus magnetic field, T-h, phase diagram [50,52,53]. The temperature, $T \sim J^{ab}$, sets the energy scale at which 3D quantum criticality for $T < J^{ab}$ crosses over to 1D behavior for $T > J^{ab}$. Similarly the three-dimensional magnetically ordered phase found for $h > h_c$ and $T = 0$ crosses over to a gapless Tomonaga-Luttinger liquid (TLL) at temperatures $T > J^{ab}$. We note that, strictly speaking, the TLL behavior should only occur [54] in the range $J^{ab} < T < J^c$, since at too large temperatures, $T \gg J^c$, classical behavior sets in. In the presence of a nonzero and small D^*, with $D^* \ll J^c$, the lowest triplet state is split into a $j = \pm 1$ doublet with energy $\Delta_\pm$ above the ground state and a $j = 0$ singlet at energy Δ_0 with $\Delta_\pm < \Delta_0$. Hence, under an applied magnetic field $\Delta_\pm$ is suppressed and the transition from the Haldane phase to the 3D ordered phase occurs around $h_c = \Delta_\pm < \Delta_s$. Apart from the downward shift of h_c, we can expect, qualitatively, a similar T-h phase diagram as in the case with no single-spin anisotropy, $D^* = 0$.

VI. CONCLUSIONS

We have analyzed the magnetic properties of the trinuclear organometallic materials, such as $Mo_3S_7(dmit)_3$. These materials are potential candidates for realizing compass interactions in their layers. In order to explore such possibilities we have derived an effective magnetic model describing the magnetic interactions between the pseudospin-one at each molecular cluster arising from strong Coulomb repulsion, lattice structure, and SMOC. In spite of the crystals being nearly isotropic, we find that the exchange coupling between nearest-neighbor pseudospins along the c direction is much larger than between pseudospins within the hexagonal a-b planes. Hence, the spin exchange model for these crystals is effectively quasi-one-dimensional. Magnetic anisotropies are found to arise under the simultaneous effect of spin orbit coupling and intracluster exchange interaction. These anisotropies are further enhanced by SMOC anisotropy, particularly when $\lambda_{xy} < \lambda_z$, which is naturally present in organometallics. Our analysis suggests that $Mo_3S_7(dmit)_3$ is most probably in the Haldane phase since the effective model consists of weakly coupled $S = 1$ antiferromagnetic chains in the presence of small single-spin anisotropy induced by SMOC. However, by increasing the interlayer distances through changes in the chemistry of the material, increasing the anisotropy of magnitude of the SMOC it should be possible to effectively drive it into the D phase. A larger SMOC should be realized in complexes containing heavier metals [12].

The Haldane phase is strongly sensitive to an external magnetic field. Under applied magnetic fields larger than the Haldane gap, $h > h_c \sim \Delta_s$, the Haldane phase is destroyed and a three-dimensional magnet may be stabilized. We have estimated this critical field h_c, based on our present analysis using DFT parameters [13] for $Mo_3S_7(dmit)_3$ (Table I) with an onsite $U = 10t_c$ and $J_F = -0.3t_c$. Using these parameters we extract $J^c = 0.0126$ eV from our Fig. 10(b) which leads to a critical magnetic field $h_c \sim \Delta_s \sim 41.4$ T assuming the Haldane spin gap, $\Delta_s = 0.414J^c \approx 0.09t_c$, in the pure Haldane chain. However, recent DMRG calculations on Hubbard tubes [27] have shown that charge fluctuations strongly suppress the spin gap when decreasing U. For the parameter range considered here, we would find $\Delta_s \sim 0.006t_c$, implying experimentally accessible critical fields: $h_c \sim 3$ T. A V-shaped quantum critical region in the T-h phase diagram separating the Haldane phase from the three-dimensional magnetically ordered phase should then emerge as observed in inorganic Haldane chain materials [53].

Exfoliation or growth of a monolayer of trinuclear complexes arranged as in the a-b planes of $Mo_3S_7(dmit)_3$, would lead to the realization of a decorated hexagonal lattice which is known to contain rich physics. We have found that at large U and no SMOC, the magnetic interactions between the pseudospin-one would be that of a conventional nearest-neighbor antiferromagnetic Heisenberg model on an hexagonal lattice [55]. The ground state of this model is a

pure Néel antiferromagnet. However, if crystal parameters are tuned so that magnetic exchange anisotropies are enhanced, disordered spin liquid phases [56] may be achieved. For instance, if the relative orientation between the molecules in the crystal is modified so that inversion symmetry within the planes is broken, a DM interaction arises [15] which competes with the magnetic order [57], which can lead to interesting spin liquid phases [58]. All this illustrates how isolated layers of trinuclear organometallic complexes are ideal playgrounds to explore the quantum many-body phases realized in a decorated honeycomb lattice.

ACKNOWLEDGMENTS

J.M. acknowledges financial support from (Grant No. MAT2015-66128-R) MINECO/FEDER, Unión Europea. Work at the University of Queensland was supported by the Australian Research Council (Grants No. FT13010016 and No. DP160100060) and by computational resources provided by the Australian Government through Raijin under the National Computational Merit Allocation Scheme.

APPENDIX A: ELECTRONIC STRUCTURE OF ISOLATED TRIANGULAR CLUSTERS

Here, we provide the details of the electronic structure of isolated clusters with different numbers of electrons.

1. Isolated triangular cluster with five electrons

We start studying isolated trimers with $N = 1$ electrons. This is due to its intrinsic importance and due to the fact that the electronic structure of trimers with $N = 5$ electrons and $t_c,\lambda_{xy},\lambda_z > 0$, relevant to $Mo_3S_7(dmit)_3$ can be obtained from the $N = 1$ case by a particle-hole transformation switching the sign of the parameters: $t_c \to -t_c,\lambda_{xy} \to -\lambda_{xy},\lambda_z \to -\lambda_z$ apart from a rigid energy shift.

For only one electron in the cluster, $N = 1$, the Hamiltonian is just $H = H_0 + H_{\rm SMOC}$. Since $[H,J_z] = 0$, where $J_z = L_z + S_z$, then the projection of the total momentum along the z axis is a good quantum number. In the following we denote the basis states for a fixed number of particles N as $|N;j,n\rangle$ where $j = k + \sigma$ and n numbers the different possible configurations for each j sector. Hence, in this case the possible basis states are

$$\begin{aligned} |1;1/2,1\rangle &= b^\dagger_{0\uparrow}|0\rangle, \quad |1;1/2,2\rangle = b^\dagger_{1\downarrow}|0\rangle, \\ |1;-1/2,1\rangle &= b^\dagger_{0\downarrow}|0\rangle, \quad |1;-1/2,2\rangle = b^\dagger_{-1\uparrow}|0\rangle, \\ |1;3/2,1\rangle &= b^\dagger_{1\uparrow}|0\rangle, \quad |1;-3/2,1\rangle = b^\dagger_{-1\downarrow}|0\rangle. \end{aligned} \tag{A1}$$

The eigenenergies, $E_n(N;j)$ of the Hamiltonian, are

$$\begin{aligned} E_2(1;j = \pm 3/2) &= t_c + \frac{\lambda_z}{2}, \\ E_1(1;j = \pm 1/2) &= -\frac{\lambda_z}{4} - \frac{t_c}{2} + \sqrt{\left(\frac{\lambda_z - 6t_c}{4}\right)^2 + \frac{\lambda_{xy}^2}{2}}, \\ E_0(1;j = \pm 1/2) &= -\frac{\lambda_z}{4} - \frac{t_c}{2} - \sqrt{\left(\frac{\lambda_z - 6t_c}{4}\right)^2 + \frac{\lambda_{xy}^2}{2}}. \end{aligned} \tag{A2}$$

Hence the level spectra for $N = 1$ consists of three doublets with the energies given above. The ground state of the system with one electron, $N = 1$, is a doublet with energy E_0. Time-reversal invariance of the Hamiltonian, $[T,H] = 0$, and Kramers theorem ensures that all states should have a minimum degeneracy of two since the cluster has an odd number of electrons. Note that the level spectra of the triangular cluster with $N = 5$ electrons (one hole) would be the same as (A2) but with the signs reversed: $t_c \to -t_c$, $\lambda_{xy} \to -\lambda_{xy},\lambda_z \to -\lambda_z$, and with an upward rigid shift of all energies by $+2U$.

To make contact with previous work on transition metal oxides it is illustrative to consider our model Hamiltonian: $H = H_0 + H_{\rm SMOC} + H_{U-J_F}$, with H_0, $H_{\rm SMOC}$ and H_{U-J_F} expressed in the (k,σ) basis as given by Eqs. (12), (14), and (16), respectively. For $U,J_F = 0$, this model is reminiscent of a model previously considered [4–6] for Ir^{4+} ions in A_2IrO_3 (A = Na,Li) compounds. In these systems, five electrons occupy the lowest t_{2g} manifold of the Ir ions which is well separated from the high energy e_g doublet. The low energy effective model for the hole in the t_{2g} manifold of the *isolated* Ir ions includes a trigonal crystal field resulting from the surrounding oxygen octahedra and a large SOC contribution [6]: $H = \Delta(L^z)^2 + \lambda \mathbf{L}\cdot\mathbf{S}$, with $\Delta > 0$. Note that in contrast to the molecular case, the SOC is isotropic, $\lambda = \lambda_{xy} = \lambda_z$, in the case of ions and atoms.

Through the particle-hole transformation discussed above, the threefold degenerate t_{2g} manifold of the isolated Ir ion with one hole is equivalent to our model of the isolated molecule with one electron, $N = 1$, with the signs of $\lambda = \lambda_{xy} = \lambda_z$ and t_c reversed. Full rotational symmetry is only recovered for $t_c \to 0$ in our model when $U,J_F = 0$. In that case, $[H_0 + H_{\rm SMOC},L] = 0$, so that the total angular momentum L is a good quantum number, as it should. In this situation, we find that isotropic SOC ($\lambda_{xy} = \lambda_z = \lambda$) splits the $(2L+1)(2S+1) = 6$ manifold ($L = 1,S = 1/2$) into a $j = 1/2$ doublet with energy $E_0(1;j = 1/2) = -\lambda$ and a $j = 3/2$ quadruplet with energy $E_1(1;j = 3/2) = \frac{\lambda}{2}$. This situation corresponds to removing the crystal field acting on the d-orbital manifold in transition metal oxides.

2. Isolated triangular clusters with four electrons

The basis states with $N = N_\uparrow + N_\downarrow = 4$ electrons includes states with total spin $S_z = 0$, ($N_\uparrow = 2,N_\downarrow = 2$), $S_z = 1$ ($N_\uparrow = 3,N_\downarrow = 1$), and $S_z = -1$ ($N_\uparrow = 1,N_\downarrow = 3$). Noting that basis states with total momentum k' are equivalent to k if they satisfy $k = k' \pm 3n$, we find that the basis states can be classified according to three possible values: $j = 0,\pm 1$. Since the Hamiltonian does not mix sates with different j, the original 15×15 matrix can be expressed in block diagonal form consisting of 5×5 matrices corresponding to $j = 0,\pm 1$. We now explicitly show the classification of the (k,σ) basis states according to $j = 0,\pm 1$ and the analytical diagonalization of the matrices corresponding to each of the j sectors. We keep the $|N;j,n\rangle$ classification of the basis states.

a. $j = 0$ *sector*

The three possible configurations with $k = \sigma = 0$ are

$$|4;0,1\rangle = b^\dagger_{0\uparrow}b^\dagger_{-1\uparrow}b^\dagger_{0\downarrow}b^\dagger_{1\downarrow}|0\rangle, \quad |4;0,2\rangle = b^\dagger_{0\uparrow}b^\dagger_{1\uparrow}b^\dagger_{0\downarrow}b^\dagger_{-1\downarrow}|0\rangle, \quad |4;0,3\rangle = b^\dagger_{-1\uparrow}b^\dagger_{1\uparrow}b^\dagger_{-1\downarrow}b^\dagger_{1\downarrow}|0\rangle. \tag{A3}$$

There is only one configuration for either $k = -1, \sigma = 1$,

$$|4;0,4\rangle = b^\dagger_{0\uparrow}b^\dagger_{-1\uparrow}b^\dagger_{1\uparrow}b^\dagger_{-1\downarrow}|0\rangle, \tag{A4}$$

or $k = 1, \sigma = -1$,

$$|4;0,5\rangle = b^\dagger_{1\uparrow}b^\dagger_{0\downarrow}b^\dagger_{-1\downarrow}b^\dagger_{1\downarrow}|0\rangle. \tag{A5}$$

Hence, the $j = 0$ Hamiltonian reduces to a 5×5 matrix:

$$H(4;j=0) = \begin{bmatrix} -2t_c + \frac{4U}{3} - \frac{7J_F}{6} - \lambda z & \frac{U-J_F/2}{3} & -\frac{U+J_F}{3} & 0 & 0 \\ \frac{U-J_F/2}{3} & -2t_c + \frac{4U}{3} - \frac{7J_F}{6} + \lambda_z & -\frac{U+J_F}{3} & -\frac{\lambda_{xy}}{\sqrt{2}} & \frac{\lambda_{xy}}{\sqrt{2}} \\ -\frac{U+J_F}{3} & -\frac{U+J_F}{3} & 4t_c + \frac{4U}{3} - \frac{5J_F}{3} & \frac{\lambda_{xy}}{\sqrt{2}} & -\frac{\lambda_{xy}}{\sqrt{2}} \\ 0 & -\frac{\lambda_{xy}}{\sqrt{2}} & \frac{\lambda_{xy}}{\sqrt{2}} & U + t_c - J_F + \frac{\lambda_z}{2} & 0 \\ 0 & \frac{\lambda_{xy}}{\sqrt{2}} & -\frac{\lambda_{xy}}{\sqrt{2}} & 0 & U + t_c - J_F + \frac{\lambda_z}{2} \end{bmatrix}.$$

b. $j = -1$ *sector*

We work in the basis,

$$\begin{aligned} &|4;-1,1\rangle = b^\dagger_{0\uparrow}b^\dagger_{-1\uparrow}b^\dagger_{-1\downarrow}b^\dagger_{1\downarrow}|0\rangle, \quad |4;-1,2\rangle = b^\dagger_{-1\uparrow}b^\dagger_{1\uparrow}b_{0\downarrow}b_{-1\downarrow}|0\rangle, \quad |4;-1,3\rangle = b^\dagger_{0\uparrow}b^\dagger_{1\uparrow}b^\dagger_{0\downarrow}b^\dagger_{1\downarrow}|0\rangle, \\ &|4;-1,4\rangle = b^\dagger_{0\uparrow}b^\dagger_{0\downarrow}b^\dagger_{-1\downarrow}b^\dagger_{1\downarrow}|0\rangle, \quad |4;-1,5\rangle = b^\dagger_{0\uparrow}b^\dagger_{-1\uparrow}b^\dagger_{1\uparrow}b^\dagger_{1\downarrow}|0\rangle. \end{aligned} \tag{A6}$$

The first three states have $k = -1 = 2, \sigma = 0$, the fourth has $k = 0, \sigma = -1$, and the fifth has $k = 1 = -2, \sigma = 1$. The $j = -1$ Hamiltonian is

$$H(4;j=-1) = \begin{bmatrix} t_c + \frac{4U}{3} - \frac{7J_F}{6} - \frac{\lambda_z}{2} & \frac{U-J_F/2}{3} & \frac{U+J_F}{3} & -\frac{\lambda_{xy}}{\sqrt{2}} & 0 \\ \frac{U-J_F/2}{3} & t_c + \frac{4U}{3} - \frac{7J_F}{6} + \frac{\lambda_z}{2} & \frac{U+J_F}{3} & 0 & 0 \\ \frac{U+J_F}{3} & \frac{U+J_F}{3} & -2t_c + \frac{4U}{3} - \frac{5J_F}{3} & 0 & -\frac{\lambda_{xy}}{\sqrt{2}} \\ -\frac{\lambda_{xy}}{\sqrt{2}} & 0 & 0 & -2t_c + U - J_F & 0 \\ 0 & 0 & -\frac{\lambda_{xy}}{\sqrt{2}} & 0 & U + t_c - J_F - \frac{\lambda_z}{2} \end{bmatrix}. \tag{A7}$$

c. $j = +1$ *sector*

It is convenient to take the basis states as the time-reversed analogs of the $j = -1$ sector:

$$\begin{aligned} &|4;+1,1\rangle = b^\dagger_{0\uparrow}b^\dagger_{1\uparrow}b^\dagger_{-1\downarrow}b^\dagger_{1\downarrow}|0\rangle, \quad |4;+1,2\rangle = b^\dagger_{-1\uparrow}b^\dagger_{1\uparrow}b^\dagger_{0\downarrow}b^\dagger_{1\downarrow}|0\rangle, \quad |4;+1,3\rangle = b^\dagger_{0\uparrow}b^\dagger_{-1\uparrow}b^\dagger_{0\downarrow}b^\dagger_{-1\downarrow}|0\rangle, \\ &|4;+1,4\rangle = b^\dagger_{0\uparrow}b^\dagger_{-1\uparrow}b^\dagger_{1\uparrow}b^\dagger_{0\downarrow}|0\rangle, \quad |4;+1,5\rangle = b^\dagger_{-1\uparrow}b^\dagger_{0\downarrow}b^\dagger_{-1\downarrow}b^\dagger_{1\downarrow}|0\rangle. \end{aligned} \tag{A8}$$

Thus one immediately sees that $H(4;j=+1) = H(4;j=-1)$. Hence, there is a double degeneracy of the eigenvalues $E_i(4;j=+1) = E_i(4;j=-1)$.

For $\lambda = 0$, the ground state is threefold degenerate corresponding to the $S = 1$ triplet combination of the two unpaired spins in the cluster. These lowest three degenerate states correspond to $j = 0, \pm 1$. From the above analysis we conclude that isolated clusters with four electrons can be described through the effective Hamiltonian given in Eq. (17) where D is an increasing function of SMOC as discussed in the main text.

3. Isolated triangular clusters with three electrons

The basis for $N = 3$ electrons consists of 20 configurations: 18 configurations with $S_z = 1/2$ ($N_\uparrow = 2, N_\downarrow = 1$) or $S_z = -1/2$ ($N_\uparrow = 1, N_\downarrow = 2$) and two configurations with $S_z = 3/2$ ($N_\uparrow = 3, N_\downarrow = 0$) or $S_z = -3/2$ ($N_\uparrow = 0, N_\downarrow = 3$). The only allowed j values for the cluster with $N = 3$ electrons are $j = \pm\frac{1}{2}, +\frac{3}{2}$ with the largest (8×8) matrix corresponding to $j = +\frac{3}{2}$. The $j = -\frac{3}{2}$ sector is not given here since the configurations are just the same as the ones in the $j = +\frac{3}{2}$ sector.

a. $j = +3/2$

The configurations with $j = 3/2$ are

$$|3;+3/2,1\rangle = b^\dagger_{0\uparrow}b^\dagger_{1\uparrow}b^\dagger_{0\downarrow}|0\rangle,\quad |3;+3/2,2\rangle = b^\dagger_{0\uparrow}b^\dagger_{-1\uparrow}b^\dagger_{-1\downarrow}|0\rangle,\quad |3;+3/2,3\rangle = b^\dagger_{-1\uparrow}b^\dagger_{1\uparrow}b^\dagger_{1\downarrow}|0\rangle,\quad |3;+3/2,4\rangle = b^\dagger_{1\uparrow}b^\dagger_{0\downarrow}b^\dagger_{1\downarrow}|0\rangle,$$
$$|3;+3/2,5\rangle = b^\dagger_{0\uparrow}b^\dagger_{-1\uparrow}b^\dagger_{1\uparrow}|0\rangle,\quad |3;+3/2,6\rangle = b^\dagger_{0\uparrow}b^\dagger_{0\downarrow}b^\dagger_{-1\downarrow}|0\rangle,\quad |3;+3/2,7\rangle = b^\dagger_{-1\uparrow}b^\dagger_{-1\downarrow}b^\dagger_{1\downarrow}|0\rangle,\quad |3;+3/2,8\rangle = b^\dagger_{0\downarrow}b^\dagger_{-1\downarrow}b^\dagger_{1\downarrow}|0\rangle. \tag{A9}$$

Yielding the 8×8 Hamiltonian matrix,

$$H(3;3/2) = \begin{bmatrix}
-3t_c+\frac{2U-5J_F/2}{3}+\frac{\lambda_z}{2} & \frac{U+J_F}{3} & \frac{U+J_F}{3} & -\frac{\lambda_{xy}}{\sqrt{2}} & -\frac{\lambda_{xy}}{\sqrt{2}} & 0 & 0 & 0\\
\frac{U+J_F}{3} & \frac{2U-5J_F/2}{3} & -\frac{U+J_F}{3} & 0 & 0 & \frac{\lambda_{xy}}{\sqrt{2}} & -\frac{\lambda_{xy}}{\sqrt{2}} & 0\\
\frac{U+J_F}{3} & -\frac{U+J_F}{3} & 3t_c+\frac{2U-5J_F/2}{3}-\frac{\lambda_z}{2} & -\frac{\lambda_{xy}}{\sqrt{2}} & -\frac{\lambda_{xy}}{\sqrt{2}} & 0 & 0 & 0\\
-\frac{\lambda_{xy}}{\sqrt{2}} & 0 & -\frac{\lambda_{xy}}{\sqrt{2}} & \frac{2U-5J_F/2}{3} & 0 & \frac{U+J_F}{3} & \frac{U+J_F}{3} & 0\\
-\frac{\lambda_{xy}}{\sqrt{2}} & 0 & -\frac{\lambda_{xy}}{\sqrt{2}} & 0 & 0 & 0 & 0 & 0\\
0 & \frac{\lambda_{xy}}{\sqrt{2}} & 0 & \frac{U+J_F}{3} & 0 & -3t_c+\frac{2U-5J_F/2}{3}+\frac{\lambda_z}{2} & -\frac{U+J_F}{3} & -\frac{\lambda_{xy}}{\sqrt{2}}\\
0 & -\frac{\lambda_{xy}}{\sqrt{2}} & 0 & \frac{U+J_F}{3} & 0 & -\frac{U+J_F}{3} & 3t_c+\frac{2U-5J_F/2}{3}-\frac{\lambda_z}{2} & \frac{\lambda_{xy}}{\sqrt{2}}\\
0 & 0 & 0 & 0 & 0 & -\frac{\lambda_{xy}}{\sqrt{2}} & \frac{\lambda_{xy}}{\sqrt{2}} & 0
\end{bmatrix}. \tag{A10}$$

b. $j = \pm 1/2$

We take the basis,

$$|3;+1/2,1\rangle = b^\dagger_{0\uparrow}b^\dagger_{0\downarrow}b^\dagger_{1\downarrow}|0\rangle,\quad |3;+1/2,2\rangle = b^\dagger_{1\uparrow}b^\dagger_{-1\downarrow}b^\dagger_{1\downarrow}|0\rangle,\quad |3;+1/2,3\rangle = b^\dagger_{-1\uparrow}b^\dagger_{0\downarrow}b^\dagger_{-1\downarrow}|0\rangle,$$
$$|3;+1/2,4\rangle = b^\dagger_{-1\uparrow}b^\dagger_{1\uparrow}b^\dagger_{0\downarrow}|0\rangle,\quad |3;+1/2,5\rangle = b^\dagger_{0\uparrow}b^\dagger_{1\uparrow}b^\dagger_{-1\downarrow}|0\rangle,\quad |3;+1/2,6\rangle = b^\dagger_{0\uparrow}b^\dagger_{-1\uparrow}b^\dagger_{1\downarrow}|0\rangle, \tag{A11}$$

and analogously for $j = -1/2$. The 6×6 Hamiltonian matrix reads

$$H(3;j=+1/2) = \begin{bmatrix}
-3t_c+\frac{2U}{3}-\frac{5J_F}{6}-\frac{\lambda_z}{2} & \frac{U+J_F}{3} & \frac{U+J_F}{3} & 0 & 0 & \frac{\lambda_{xy}}{\sqrt{2}}\\
\frac{U+J_F}{3} & 3t_c+\frac{2U}{3}-\frac{5J_F}{6}+\frac{\lambda_z}{2} & -\frac{U+J_F}{3} & 0 & -\frac{\lambda_{xy}}{\sqrt{2}} & 0\\
\frac{U+J_F}{3} & -\frac{U+J_F}{3} & \frac{2U}{3}-\frac{5J_F}{6} & 0 & 0 & 0\\
0 & 0 & 0 & \frac{2U}{3}-\frac{J_F}{3} & \frac{U-J_F/2}{3} & -\frac{U-J_F/2}{3}\\
0 & -\frac{\lambda_{xy}}{\sqrt{2}} & 0 & \frac{U-J_F/2}{3} & \frac{2U}{3}-J_F/3+\lambda_z & \frac{U-J_F/2}{3}\\
\frac{\lambda_{xy}}{\sqrt{2}} & 0 & 0 & -\frac{U-J_F/2}{3} & \frac{U-J_F/2}{3} & \frac{2U}{3}-\frac{J_F}{3}-\lambda_z
\end{bmatrix}.$$

Due to Kramers theorem the eigenstates, $E_n(3;j=1/2) = E_n(3;j=-1/2)$ and the energy levels for $E_n(3;j=3/2)$ are at least doubly degenerate. With no SMOC present, $E_n(3;j=\pm 1/2) = E_n(3;j=3/2)$ and the eigenstates are fourfold degenerate. However, when SMOC is present $E_n(3;j=\pm 1/2) \neq E_n(3;j=3/2)$ and the fourfold degeneracy is broken leading to twofold degenerate levels.

APPENDIX B: EXPRESSION FOR EFFECTIVE SPIN MODELS FROM THE CANONICAL TRANSFORMATION OF THE *t*-*J* MODEL

In this Appendix we model the ℓth trinuclear complex by the three site t-J model, i.e.,

$$H^{(\ell)}_{t-J} \equiv P_0\left[\sum_{\sigma,j=1}^{3} t_c(h^\dagger_{\ell j\sigma}h_{\ell(j+1)\sigma} + h^\dagger_{\ell j\sigma}h_{\ell(j-1)\sigma}) - \frac{J_c}{4}\sum_{i\neq j\neq k=1}^{3}\sum_{\sigma,\sigma'} h_{\ell i\sigma}h^\dagger_{\ell j\sigma}(1-n_{\ell j\uparrow})(1-n_{\ell j\downarrow})a_{\ell j\sigma'}a^\dagger_{\ell k\sigma'}\right]P_0, \tag{B1}$$

where $h^\dagger_{\ell i\sigma} = a_{\ell i\sigma}$ creates a hole with spin σ in the ith Wannier orbital and P_0 projects out states that contain empty sites. Note that it is important to retain the "three site" terms here, as we will need to consider states far from half-filling. For a single molecule the effective low-energy model, retaining only the three lowest energy states is given by Eq. (17) with

$$D = \frac{\lambda_z^2-\lambda_{xy}^2}{6(2t_c-J_c)}. \tag{B2}$$

The t-J model of the interlayer coupling between neighboring molecules ℓ and m is

$$H^c_{t-J} = P_0\left[-t_z\sum_\sigma\sum_{j=1}^{3}(h^\dagger_{\ell j\sigma}h_{mj\sigma}+h^\dagger_{mj\sigma}h_{\ell j\sigma})+J_z\sum_{j=1}^{3}\left(\hat{\boldsymbol{S}}_{\ell j}\cdot\hat{\boldsymbol{S}}_{mj}-\frac{\hat{n}_{\ell j}\hat{n}_{mj}}{4}\right)\right]P_0, \tag{B3}$$

where now there are no three site terms because of the topology of the underlying tight-binding model [cf. Eq. (21) and Fig. 2(b)]. Performing the canonical transformation described in Sec. IV A and retaining quadratic terms in t_z, linear terms in J_z (as J_z is already quadratic in t_z) and quadratic terms in the SMOC (i.e., up to order λ_z^2, λ_{xy}^2, or $\lambda_{xy}\lambda_z$) yields an effective Hamiltonian described by Eq. (33) with

$$\Delta D^c = -\frac{t_z^2}{81}\left[\frac{28t_c+J_c}{(2t_c-J_c)^3t_c}\lambda_z^2-\frac{24J_ct_c^3+29J_c^2t_c^2-17J_c^3t_c+2J_c^4}{2(4t_c-J_c)(2t_c-J_c)^3t_c^3}\lambda_{xy}^2\right], \tag{B4a}$$

$$J^c = \frac{J_z}{3}\left[1-\frac{1}{12(2t_c-J_c)^2}\lambda_z^2-\frac{J_c^2}{48(2t_c-J_c)^2t_c^2}\lambda_{xy}^2\right] + \frac{t_z^2}{81}\frac{36}{2t_c-J_c}\left[1+\frac{2}{9(2t_c-J_c)^2}\lambda_z^2-\frac{160t_c^4-48J_ct_c^3-52J_c^2t_c^2+26J_c^3t_c-3J_c^4}{72(4t_c-J_c)(2t_c-J_c)^2t_c^3}\lambda_{xy}^2\right], \tag{B4b}$$

$$\Delta^c = 1+\frac{J_z}{48(2t_c-J_c)t_z^2}\left(7\lambda_z^2+\frac{48J_ct_c^3-12J_c^2t_c^2-9J_c^3t_c+2J_c^4}{4(4t_c-J_c)t_c^3}\lambda_{xy}^2\right) - \frac{1}{9(2t_c-J_c)^2}\left[\lambda_z^2+\frac{24J_ct_c^3-6J_c^3t_c+J_c^4}{8(4t_c-J_c)t_c^3}\lambda_{xy}^2\right], \tag{B4c}$$

$$P_{zz} = \frac{4t_z^2}{9(2t_c-J_c)^3}\lambda_z^2, \tag{B4d}$$

$$P_{xx} = \frac{t_z^2}{81}\frac{J_c^2(5t_c-J_c)}{(2t_c-J_c)^3t_c^3}\lambda_{xy}^2, \tag{B4e}$$

$$P_{zx} = \frac{P_{xx}+P_{zz}}{2}. \tag{B4f}$$

The t-J model of the in-plane coupling between molecules ℓ and m along a "1-bond" (cf. Fig. 1) is

$$H^{ab}_{t-J} = -t_g\sum_\sigma P_0(\hat{a}^\dagger_{\ell1\sigma}\hat{a}_{m1\sigma}+\hat{a}^\dagger_{m1\sigma}\hat{a}_{\ell1\sigma})P_0+J_cP_0\left(\boldsymbol{S}_{\ell1}\cdot\boldsymbol{S}_{m1}-\frac{\hat{n}_{\ell1}\hat{n}_{m1}}{4}\right)P_0, \tag{B5}$$

again the three site terms vanish because of the underlying tight-binding model [Eq. (19)]. Performing the canonical transformation, adding in the 2- and 3-bonds, as described in Sec. IV A, and retaining quadratic terms in t_g, linear terms in J_g, and quadratic terms in the SMOC yields an effective Hamiltonian described by Eq. (36) with

$$\Delta D^{ab} = -\frac{t_g^2}{81}\left[\frac{30t_c^2-16J_ct_c+2J_c^2}{9(4t_c-J_c)(2t_c-J_c)^2t_c^2}\lambda_z^2-\frac{96J_ct_c^3-212J_c^2t_c^2+90J_c^3t_c-11J_c^4}{36(4t_c-J_c)(2t_c-J_c)^3t_c^3}\lambda_{xy}^2\right], \tag{B6a}$$

$$J^{ab} = \frac{J_g}{9}\left[1-\frac{\lambda_z^2}{12(2t_c-J_c)^2}-\frac{J_c^2\lambda_{xy}^2}{48(2t_c-J_c)^2t_c^2}\right] + \frac{t_g^2}{81}\frac{4J_c}{t_c(2t_c-J_c)}\left[1+\frac{(5t_c^2-5t_cJ_c+J_c^2)}{36(2t_c-J_c)^2}\frac{\lambda_z^2}{t_c^2}-\frac{240t_c^3-190J_ct_c^2+53J_c^2t_c-5J_c^3}{36(4t_c-J_c)(2t_c-J_c)^2}\frac{\lambda_{xy}^2}{t_c^2}\right], \tag{B6b}$$

$$Q = \left[\frac{J_g}{9}\frac{J_c(8t_c+5J_c)}{144(2t_c-J_c)^2}-\frac{t_g^2}{81}\frac{48t_c^2J_c-26t_cJ_c^2+3J_c^3}{18t_c(2t_c-J_c)^2(4t_c-J_c)}\right]\frac{\lambda_{xy}^2}{t_c^2}, \tag{B6c}$$

$$\Delta^{ab} = 1-\frac{J_g}{16J_c(2t_c-J_c)t_g^2}\left[(4t_c-J_c)\lambda_z^2-\frac{384t_c^3-152J_ct_c^2+3J_c^3}{4(4t_c-J_c)t_c}\lambda_{xy}^2\right] + \frac{1}{36(J_c-2t_c)^2t_c}\left[(7t_c-J_c)\lambda_z^2-\frac{96t_c^2-38J_ct_c+3J_c^2}{4t_c-J_c}\lambda_{xy}^2\right], \tag{B6d}$$

$$J^{ab}_{xz} = \frac{1}{\sqrt{2}}\left[-\frac{J_g}{9}\left(\frac{J_c}{36(2t_c-J_c)^2t_c}\right)+\frac{t_g^2}{81}\left(\frac{J_c(12t_c^2-6J_ct_c^2+J_c^2)}{9(4t_c-J_c)(2t_c-J_c)^3t_c^2}\right)\right]\lambda_{xy}\lambda_z. \tag{B6e}$$

[1] W. Witczak-Krempa, G. Chen, Y. B. Kim, and L. Balents, Annu. Rev. Condens. Matter Phys. **5**, 57 (2014).
[2] D. Pesin and L. Balents, Nat. Phys. **6**, 376 (2010).
[3] Z. Nussinov and J. van den Brink, Rev. Mod. Phys. **87**, 1 (2015).
[4] G. Jackeli and G. Khaliullin, Phys. Rev. Lett. **102**, 017205 (2009).
[5] N. B. Perkins, Y. Sizyuk, and P. Wölfle, Phys. Rev. B **89**, 035143 (2014).
[6] Y. Sizyuk, C. Price, P. Wölfle, and N. B. Perkins, Phys. Rev. B **90**, 155126 (2014).
[7] A. Kitaev, Ann. Phys. **321**, 2 (2006).
[8] M. G. Yamada, H. Fujita, and M. Oshikawa, Phys. Rev. Lett. **119**, 057202 (2017).
[9] S. M. Winter, K. Riedl, and R. Valentí, Phys. Rev. B **95**, 060404 (2017).
[10] B. J. Powell, E. P. Kenny, and J. Merino, Phys. Rev. Lett. **119**, 087204 (2017).
[11] Y. Jiang, A. Tang, R. Hoffmann, J. Huang, and J. Lu, Organometallics **4**, 27 (1985).
[12] A. L. Khosla, A. C. Jacko, J. Merino, and B. J. Powell, Phys. Rev. B **95**, 115109 (2017).
[13] A. C. Jacko, A. L. Khosla, J. Merino, and B. J. Powell, Phys. Rev. B **95**, 155120 (2017).
[14] J. Merino, A. C. Jacko, A. L. Khosla, and B. J. Powell, Phys. Rev. B **94**, 205109 (2016).
[15] B. J. Powell, J. Merino, A. L. Khosla, and A. C. Jacko, Phys. Rev. B **95**, 094432 (2017); **96**, 099902(E) (2017).
[16] A. C. Jacko, C. Janani, K. Koepernik, and B. J. Powell, Phys. Rev. B **91**, 125140 (2015).
[17] A. Ruegg, J. Wen, and G. A. Fiete, Phys. Rev. B **81**, 205115 (2010).
[18] C. L. Kane and E. J. Mele, Phys. Rev. Lett. **95**, 146802 (2005).
[19] H. Yao and S. A. Kivelson, Phys. Rev. Lett. **99**, 247203 (2007).
[20] O. J. Silveira, S. S. Alexandre, and H. Chacham, J. Phys. Chem. C **120**, 19796 (2016).
[21] Y.-P. Wang, W.-X. Ji, C.-W. Zhang, P. Li, P.-J. Wang, B. Kong, S.-S. Li, S.-S. Yan, and K. Liang, Appl. Phys. Lett. **110**, 233107 (2017).
[22] Z. F. Wang, Z. Liu, and F. Liu, Phys. Rev. Lett. **110**, 196801 (2013).
[23] Z. F. Wang, Z. Liu, and F. Liu, Nat. Commun. **4**, 1471 (2013).
[24] J. P. Sheckelton, J. R. Neilson, D. G. Soltan, and T. M. McQueen, Nat. Mater. **11**, 493 (2012).
[25] J.-K. Bao, J.-Y. Liu, C.-W. Ma, Z.-H. Meng, Z.-T. Tang, Y.-L. Sun, H.-F. Zhai, H. Jiang, H. Bai, C.-M. Feng, Z.-A. Xu, and G.-H. Cao, Phys. Rev. X **5**, 011013 (2015).
[26] G. Chen, H.-Y. Kee, and Y. B. Kim, Phys. Rev. B **93**, 245134 (2016).
[27] H. L. Nourse, I. P. McCulloch, C. Janani, and B. J. Powell, Phys. Rev. B **94**, 214418 (2016).
[28] C. Janani, J. Merino, I. P. McCulloch, and B. J. Powell, Phys. Rev. Lett. **113**, 267204 (2014).
[29] C. Janani, J. Merino, I. P. McCulloch, and B. J. Powell, Phys. Rev. B **90**, 035120 (2014).
[30] G. Khaliullin, Prog. Theor. Phys. **160**, 155 (2005).
[31] S. Bhattacharjee, S.-S. Lee, and Y. B. Kim, New J. Phys. **14**, 073015 (2012).
[32] F. Neese, J. Chem. Phys. **122**, 034107 (2005).
[33] B. J. Powell, Coord. Chem. Rev. **295**, 46 (2015).
[34] T. Yildirim, A. B. Harris, A. Aharony, and O. Entin-Wohlman, Phys. Rev. B **52**, 10239 (1995).
[35] T. Moriya, Phys. Rev. **120**, 91 (1960).
[36] L. Shekhtman, O. Entin-Wohlman, and A. Aharony, Phys. Rev. Lett. **69**, 836 (1992).
[37] K. A. Chao, J. Spałek, and A. M. Oleś, J. Phys. C **10**, L271 (1977).
[38] A. B. Harris and R. V. Lange, Phys. Rev. **157**, 295 (1967).
[39] I. Affleck, T. Kennedy, E. H. Lieb, and H. Tasaki, Phys. Rev. Lett. **59**, 799 (1987).
[40] S. R. White and D. A. Huse, Phys. Rev. B **48**, 3844 (1993).
[41] F. D. M. Haldane, Phys. Lett. A **93**, 464 (1983).
[42] F. D. M. Haldane, Phys. Rev. Lett. **50**, 1153 (1983).
[43] G. Gómez-Santos, Phys. Rev. Lett. **63**, 790 (1989).
[44] F. Pollmann, E. Berg, A. M. Turner, and M. Oshikawa, Phys. Rev. B **85**, 075125 (2012).
[45] A. F. Albuquerque, C. J. Hamer, and J. Oitmaa, Phys. Rev. B **79**, 054412 (2009).
[46] S. Hu, B. Normand, X. Wang, and L. Yu, Phys. Rev. B **84**, 220402(R) (2011).
[47] A. Langari, F. Pollmann, and M. Siahatgar, J. Phys.: Condens. Matter **25**, 406002 (2013).
[48] Y.-C. Tzeng and M.-F. Yang, Phys. Rev. A **77**, 012311 (2008).
[49] K. Wierschem and P. Sengupta, JPS Conf. Proc. **3**, 012005 (2014).
[50] T. Sakai and M. Takahashi, Phys. Rev. B **42**, 4537 (1990).
[51] I. Affleck, Phys. Rev. B **41**, 6697 (1990).
[52] E. Orignac, R. Citro, and T. Giamarchi, Phys. Rev. B **75**, 140403 (2007).
[53] A. K. Bera, B. Lake, A. T. M. N. Islam, and A. Schneidewind, Phys. Rev. B **92**, 060412(R) (2015).
[54] M. Dupont, S. Capponi, and N. Laflorencie, Phys. Rev. B **94**, 144409 (2016).
[55] Next-nearest antiferromagnetic couplings in $Mo_3S_7(dmit)_3$ are estimated to be small, about $(t/3t_c)^2 \sim 1/15$ times the nearest-neighbor exchange couplings (see also Ref. [14] for more details).
[56] S.-S. Gong, W. Zhu, and D. N. Sheng, Phys. Rev. B **92**, 195110 (2015).
[57] O. Cepas, C. M. Fong, P. W. Leung, and C. Lhuillier, Phys. Rev. B **78**, 140405(R) (2008).
[58] L. Messio, S. Bieri, C. Lhuillier, and B. Bernu, Phys. Rev. Lett. **118**, 267201 (2017).